11 Supernovae

W. Michael Wood-Vasey, David Arnett, S. J. Asztalos, Stephen Bailey, Joseph P. Bernstein, Rahul Biswas, David Cinabro, Kem H. Cook, Jeff Cooke, Willem H. de Vries, Benjamin Dilday, Brian D. Fields, Josh Frieman, Peter Garnavich, Mario Hamuy, Saurabh W. Jha, Richard Kessler, Stephen Kuhlman, Amy Lien, Sergei Nikolaev, Masamune Oguri, Scot S. Olivier, Philip A. Pinto, Jeonghee Rho, Evan Scannapieco, Benjamin D. Wandelt, Yun Wang, Patrick Young, Hu Zhan

11.1 Introduction

Josh Frieman, W. Michael Wood-Vasey

In 1998, measurements of the Hubble diagram of Type Ia supernovae (SNe Ia) provided the first direct evidence for cosmic acceleration (Riess et al. 1998; Perlmutter et al. 1999). This discovery rested on observations of several tens of supernovae at low and high redshift. In the intervening decade, several dedicated SN Ia surveys have together measured light curves for over a thousand SNe Ia, confirming and sharpening the evidence for accelerated expansion.

Despite these advances (or perhaps because of them), a number of concerns have arisen about the robustness of current SN Ia cosmology constraints. The SN Ia Hubble diagram is constructed from combining low- and high-redshift SN Ia samples that have been observed with a variety of telescopes, instruments, and photometric passbands. Photometric offsets between these samples are degenerate with changes in cosmological parameters. In addition, the low-redshift SN Ia measurements that are used both to anchor the Hubble diagram and to train SN Ia distance estimators were themselves compiled from combinations of several surveys using different telescopes and selection criteria. When these effects are combined with uncertainties in intrinsic SN Ia color variations and in the effects of dust extinction, the result is that the current constraints are largely dominated by systematic as opposed to statistical errors.

Roughly 10^3 supernovae have been discovered in the history of astronomy. In comparison, LSST will discover over ten million supernovae during its ten-year survey, spanning a very broad range in redshift and with precise, uniform photometric calibration. This will enable a dramatic step forward in supernova studies, using the power of unprecedented large statistics to control systematic errors and thereby lead to major advances in the precision of supernova cosmology. This overwhelming compendium of stellar explosions will also allow for novel techniques and insights to be brought to bear in the study of large-scale structure, the explosion physics of supernovae of all types, and star formation and evolution. The LSST sample will include hundreds of thousands of well-measured Type Ia supernovae (SNe Ia), replicating the current generation of SN Ia cosmology experiments several hundred times over in different directions and regions across the sky, providing a stringent test of homogeneity and isotropy. Subsamples as a function of redshift, galaxy type, environment, and supernova properties will allow for detailed investigations of supernova evolution and of the relationship between supernovae and the processing of baryons in galaxies, one of the keys to understanding galaxy formation. Such large samples of supernovae, supplemented by follow-up observations, will reveal details of supernova explosions both from the large statistics of typical supernovae and the extra leverage and perspective of the outliers of the supernova population. The skewness of the brightness distribution of SNe Ia as a function of redshift will encode the lensing structure of the massive systems traversed by the SN Ia light on the way to us on Earth. There will even be enough SNe Ia to construct a SN Ia-only baryon acoustic oscillation measurement that will provide independent checks on the more precise galaxy-based method as well as allowing for a SN Ia-only constraint on $\Omega_{\rm m}$. This will allow SNe Ia alone to constrain σ_8 and $\Omega_{\rm m}$, as well as the properties of dark energy over the past 10 billion years of cosmic history. Finally, millions of supernovae will allow for population investigations using supernovae that were once reserved for large galaxy surveys (Wood-Vasey et al. 2009).

Supernovae are dynamic events that occur on time scales of hours to months, but they allow us to probe billions of years into the past. From studying nearby progenitors of these violent deaths of stars, to studying early massive stellar explosions and connecting with the star formation in between, to probing properties of host galaxies, clusters and determining the arrangement of the galaxies themselves, supernovae probe the scales of the Universe from an AU to a Hubble radius.

The standard LSST cadence of revisits every several days carried out over years, in addition to specialized "deep-drilling" fields to monitor for variations on the time scale of hours (§ 2.1), offers the perfect laboratory to study supernovae. In this chapter we consider the science possible with two complementary cadences for observations with the LSST, one based on the standard cadence of 3–4 days (the "main" survey in what follows) and another survey over a smaller area of sky using a more rapid cadence, going substantially deeper in a single epoch (the "deep" survey). As described in § 2.1, the detailed plans for the deep-drilling fields are still under discussion, but they have two potential benefits: allowing us to get improved light curve coverage for supernovae at intermediate redshifts ($z \sim 0.5$), and pushing photometry deep enough to allow SNe Ia to $z \sim 1$ to be observed. With this in mind, the ideal cadence would be repeat observations of a single field on a given night, totalling 10-20 minutes in any given band. We would return to the field each night with a different filter, thus cycling through the filters every five or six nights. Because the SNe Ia discovered in this mode will be in a small number of such deep fields, it is plausible to imagine carrying out a follow-up survey of their host galaxies with a wide-field, multi-object spectrograph to obtain spectroscopic redshifts.

The outline of this chapter is as follows. § 11.2 describes detailed simulations of SN Ia light curves for both the main and deep LSST fields and the resulting expected numbers of measured SNe Ia as a function of redshift for different selection criteria, while § 11.3 quantifies the contamination of the SN Ia sample by core-collapse supernovae. In § 11.4 we discuss photometric redshift estimation with SN Ia light curves, the expected precision of such redshift estimates, and their suitability for use in cosmological studies. § 11.5 describes the constraints on dark energy that will result from such a large SN Ia sample. The large sky coverage of the LSST SN Ia sample will enable a novel probe of large-scale homogeneity and isotropy, as described in § 11.6. § 11.7, presents the issue of SN Ia evolution, a potential systematic for SN Ia cosmology studies. In § 11.8 we discuss SN Ia rate models and the use of LSST to probe them. § 11.9 describes how SN Ia measurements can be used to measure the baryon acoustic oscillation feature in a manner complementary to that using the galaxy distribution. The effects of weak lensing on the distribution of SN Ia brightness and its possible use as a cosmological probe are described in § 11.10. We then turn to core-collapse SN, discussing their rates in § 11.12 and their use for distance measurements and cosmology in § 11.12. § 11.13 discusses the prospects for measuring SN light echoes with LSST. Pair-production SNe, the hypothetical endpoints of the evolution of supermassive stars, are the subject of § 11.14. Finally, we conclude with a discussion of the opportunities for education and outreach with LSST supernovae in § 11.15.

11.2 Simulations of SN Ia Light Curves and Event Rates

Stephen Bailey, Joseph P. Bernstein, David Cinabro, Richard Kessler, Steve Kuhlman

We begin with estimates for the anticipated SN Ia sample that LSST will observe. We put emphasis on those objects with good enough photometry that detailed light curves can be fit to them, as these are the objects that can be used in cosmological studies as described below.

SNe Ia are simulated assuming a volumetric rate of

$$r_V(z) = 2.6 \times 10^{-5}(1+z)^{1.5} \text{ SNe } h_{70}^3 \text{ Mpc}^{-3} \text{ yr}^{-1} \tag{11.1}$$

based on the rate analysis in Dilday et al. (2008). See § 11.8 for how LSST can improve the measurement of SNe Ia rates. At redshifts beyond about $z \simeq 1$, the above rate is likely an overestimate since it does not account for a correlated decrease with star formation rates at higher redshifts. We simulated one year of LSST data; thus the total numbers of SNe we present below should be multiplied by ten for the full survey.

For each observation the simulation determines the (source) flux and sky noise in photoelectrons measured by the telescope CCDs, and then estimates the total noise, assuming PSF fitting, that would be determined from an image subtraction algorithm that subtracts the host galaxy and sky background. For this initial study we have ignored additional sky noise from the deep co-added template used for the image subtraction, as well as noise from the host galaxy; we expect these effects to be small.

We use the outputs of the Operations Simulator (§ 3.1) to generate SN Ia light curves with a realistic cadence, including the effects of weather. The light curves were made by `SNANA` (Kessler et al. 2009b), a publicly available[1] simulation and light curve fitter. We carry out simulations separately for the universal cadence, and for seven deep drilling fields, which are visited in each filter on a five-day cadence (see the discussion in § 2.1).

We explore the contamination of the SN Ia sample by other types of SNe in § 11.3.

[1] http://www.sdss.org/supernova/SNANA.html

11.2.1 Light Curve Selection Criteria

A SN Ia light curve depends on a number of parameters: a stretch (shape) parameter, redshift, extinction, intrinsic color, and so on. Fitting for all these parameters requires high-quality photometric data. Here, we apply a series of cuts on the data to identify those supernovae with good enough repeat photometry of high signal-to-noise ratio (S/N) in multiple bands to allow a high-quality light curve to be fit to it. Defining $T_{\rm rest}$ as the rest-frame epoch where $T_{\rm rest} = 0$ at peak brightness, the selection requirements are

- at least one epoch with $T_{\rm rest} < -5$ days (no S/N cut);
- at least one epoch with $T_{\rm rest} > +30$ days (no S/N cut);
- at least seven different nights with one or more observations, $-20 < T_{\rm rest} < +60$ (no S/N cut);
- largest "near-peak" gap in the coverage (no S/N cut) is < 15 rest-frame days, where "near-peak" means that the gap overlaps the -5 to $+30$ day region;
- at least $N_{\rm filt}$ passbands that have a measurement with $\mathrm{S/N_{max}} > \{10, 15, 20\}$ (we explore variations in $\mathrm{S/N_{max}}$ below).
- All observations used in the cuts above satisfy $3000 < \bar{\lambda}_{\rm obs}/(1+z) < 9000$ Å, where $\bar{\lambda}_{\rm obs}$ is the mean wavelength of the observer-frame filter.

We applied no S/N requirement on the light curve sampling requirements; the S/N requirement is made only on the highest S/N value in a given number of passbands. The large temporal coverage (-5 to $+30$ days) is motivated by the necessity to reject non-Ia SNe based solely on photometric identification (see § 11.3).

11.2.2 Rate Results

Figure 11.1 compares distributions of various observables obtained from the deep drilling and main fields. As expected, the deep survey has several times more total observations per light curve than the main survey, and the deep fields probe higher redshifts. However, the number of nights with an observation (third panel down) is comparable for the deep and main surveys. The distribution of the largest time with no photometric data points is slightly narrower for the deep survey.

A total of 10^4 and 1.4×10^5 SNe Ia were generated for the deep and main surveys, respectively in a single year. Each deep field is sampled more than 1,000 times, and each main survey field is sampled about 40 times in that year. The number of SNe Ia per season after selection requirements is shown in Figure 11.2. The SN sample size is plotted as a function of $N_{\rm filt}$ for $\mathrm{S/N_{max}}$ values of 10, 15, and 20. Even with the strictest requirements of four filters with $\mathrm{S/N_{max}} > 20$, we recover 500 SNe Ia per season in the deep fields and roughly 10,000 in the main survey.

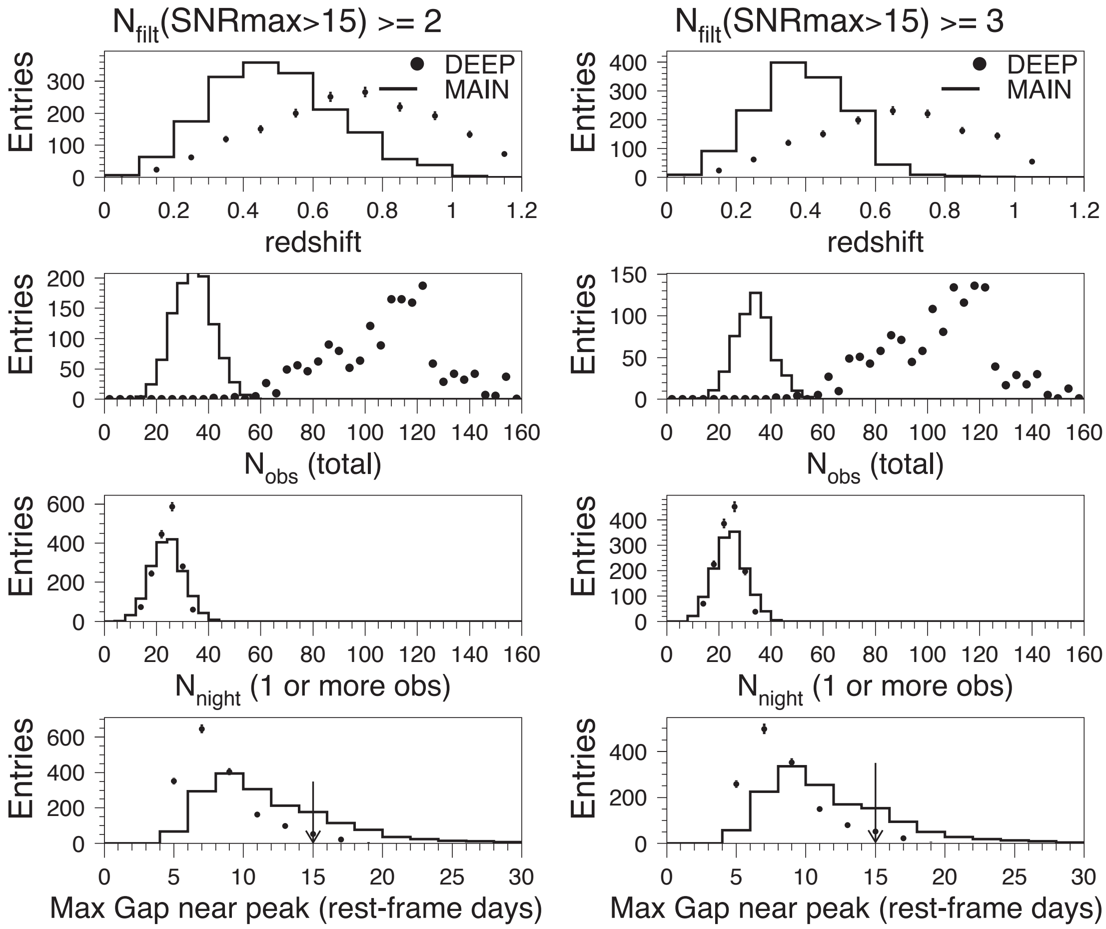

Figure 11.1: Distributions of SN Ia lightcurve characteristics for our Monte Carlo simulations of one year of the deep and main surveys, where the main field histograms have been scaled to have the same statistics as for the deep fields. The quantities shown are the redshift distribution of SN Ia (top), the total number of obervations of each supernova (summed over filters, second row), the total number of nights each object has been observed (third row; thus the ratio of N_{obs} to N_{night} is a measure of the number of observations of the supernova per night), and the largest gap in days of the coverage of the supernova. The S/N-related cut (see text) is indicated at the top of each column. All selection requirements have been applied, except for the cut on the maximum gap in the light curve in the bottom plot. The vertical arrow at 15 days shows this nominal cut.

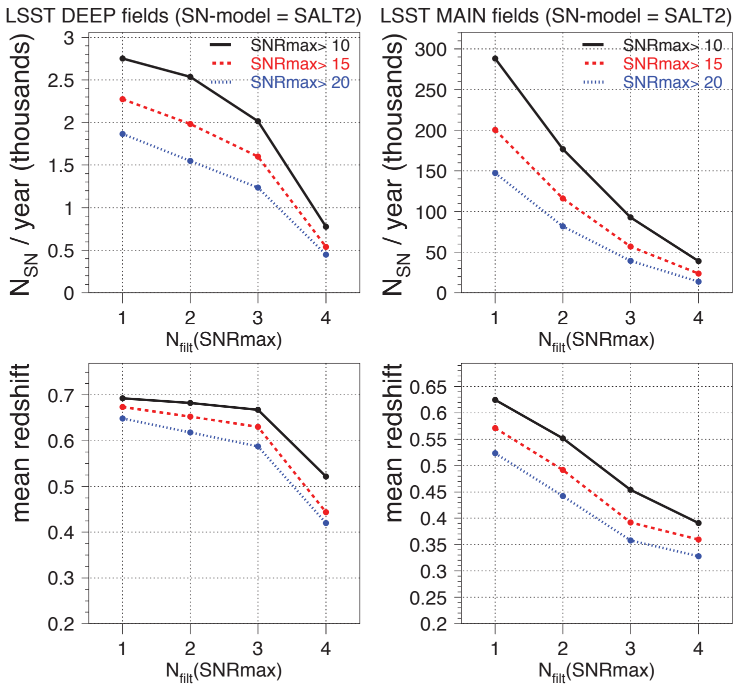

Figure 11.2: The upper panels show the number of SNe Ia detected in a single year in the deep drilling fields (left) and universal cadence fields (right) which have good enough photometry to allow fitting of a high-quality light curve, using the criteria outlined in the text, for various values of S/N_{max}. The more filters in which high-quality photometry is available, the better the resulting constraint on supernova parameters; the number of filters is shown along the x-axis. The lower panel shows the mean redshift of the resulting SNe Ia samples. These simulations use the `SALT-II` model (Guy et al. 2007) to generate light curves; we find similar results using the MLCS method (Jha et al. 2007).

11.2.3 Visual Examination of SN Light Curves

Not surprisingly, the main survey light curves are considerably sparser than for the deep survey, as shown in simulated data for the two in Figure 11.3 and Figure 11.4. All light curves satisfy the requirement $N_{\rm filt}(S/N_{max} > 15) \geq 3$ so that we have at least two well-measured colors.

For the deep fields, the excellent sampling in all passbands results in measured colors that do not require any interpolation between data points. In contrast, the main fields typically have poor sampling in any one passband, even though the combined sampling passes the selection requirements. SN 40001 (Figure 11.3, center panel), for example, has just one observation before the peak in the y-band, and hence no pre-max color measurements. SN 40004 (left panel) has a decent $y-z$ color measured near peak, but the g, r, i measurements are so far past peak that there is essentially no second color measurement near peak. Although one can introduce more ad-hoc selection requirements to ensure visually better sampling in multiple passbands, it would be better to define cuts based on how the sampling quality is related to the precision of the cosmological parameters.

Future work should include running light curve fits on large simulated SN samples to extract both

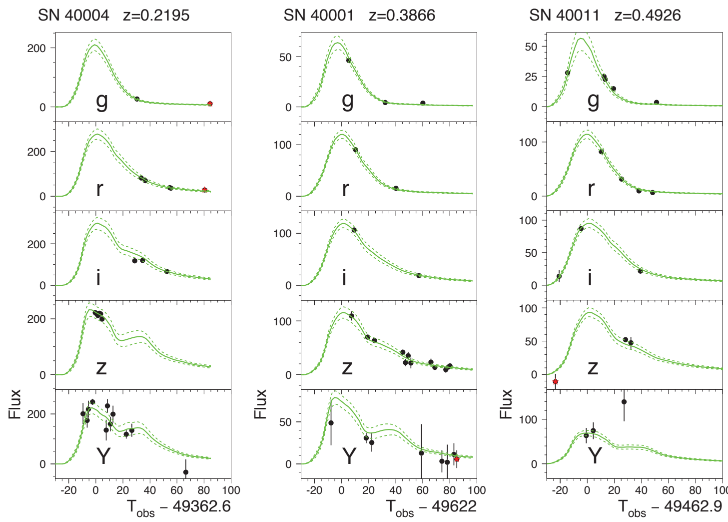

Figure 11.3: Simulated SNe Ia light curves (dots), along with the best fit model (green curve), for three representative SNe Ia from the main field that satisfy the selection requirements (§ 11.2.1) with three or more passbands having a measurement with S/N> 15. The redshift is shown above each panel. The dashed green curve represents the model error. The red stars are measurements excluded from the fit because $T_{\rm rest} < -15$ days or $T_{\rm rest} > +60$ days.

a distance modulus and redshift (i.e., a photometric redshift fit; § 11.4), and then determining the cosmological constraints, biases, and contamination. These results can then be used to optimize the light curve sampling requirements per passband.

11.3 Simulations of Core-Collapse Supernova Light Curves and Event Rates

Joseph P. Bernstein, David Cinabro, Richard Kessler, Stephen Kuhlman

Because the vast majority of SNe that LSST will observe have no spectroscopic follow-up, the scientific return from LSST SNe will be strongly dependent on the ability to use photometric typing to classify and determine redshifts for these events. In this section we consider the contamination rate of the cosmological sample of SNe Ia by core-collapse SNe. The simulations described here assume that we have spectroscopic redshifts for either the SNe or, more likely, the SN host galaxy. This is certainly not going to be the case for LSST, and these investigations need to be repeated in the context of photometric redshifts.

Light curves of core-collapse SNe (henceforth "SNcc"; i.e., SNe Ib/c and SNe II) are less standard and less comprehensively studied than are the detailed models of normal SNe Ia we used above. Therefore, we take a template approach to modeling SNcc. We utilized the following spectral templates constructed by Peter Nugent[2]:

[2] http://supernova.lbl.gov/~nugent/nugent_templates.html

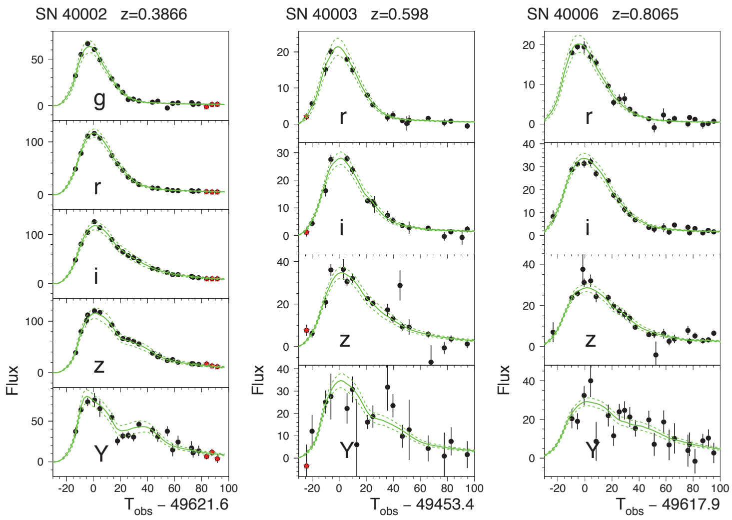

Figure 11.4: Same as for Figure 11.3, but now for the deep drilling survey. Note how much better sampled the light curves are than for the main survey fields.

- SNe Ib/c based on SN1999ex, which lies in the middle of the range defined by the three SNe discussed in Hamuy et al. (2002);
- SNe IIl from Gilliland et al. (1999);
- SNe IIn based on SN1999el as discussed in Di Carlo et al. (2002) (note however that this supernova is almost 2 magnitudes dimmer than a typical SN IIn; we have corrected this back to "normal" luminosity, which we correct for),
- composite SNe IIp based on Baron et al. (2004),

As discussed in Nugent et al. (2002), one should use caution when applying the above templates to for example, making K-corrections for determination of rates or cosmology.

These templates do not include intrinsic magnitude or color fluctuations. We added intrinsic magnitude fluctuations, coherent in all passbands, based on Richardson et al. (2002).

In order to simulate SNcc with `SNANA`, one must define the input supernova rate. Dilday et al. (2008) found the SN Ia rate from SDSS to be of the form $\alpha(1+z)^{\beta}$ with $\alpha_{Ia} = 2.6\times10^{-5}\,\mathrm{SNe\,Mpc^{-3}\,yr^{-1}}$ and $\beta_{Ia} = 1.5$. For SNcc, we take $\beta_{cc} = 3.6$ to match the observed star formation rate. Various studies, the most recent being the SuperNova Legacy Survey (SNLS) (Bazin et al. 2009), have shown this assumption to be valid, albeit with low statistics and limited redshift range. We normalize the SNcc rate using the observed ratio of cc/Ia from the SNLS survey of 4.5 at $z < 0.4$, giving $\alpha_{cc} = 6.8\times10^{-5}\,\mathrm{SNe\,Mpc^{-3}\,yr^{-1}}$. Further discussion may be found in § 11.11. The relative numbers of different types of core-collapse supernovae are poorly known. Our guesses, which we used in the simulations, are shown in Table 11.1; they are based on Mannucci et al. (2005) and Cappellaro et al. (1999) for the Ib/c's, Cappellaro et al. (1999) for SNe IIn, and private communications from Peter Nugent for SNe IIl.

Given these assumptions, we simulated a population of core-collapse objects using the `SNANA` code described in § 11.2. We then fit the simulated photometry of each object in the combined SNe Ia

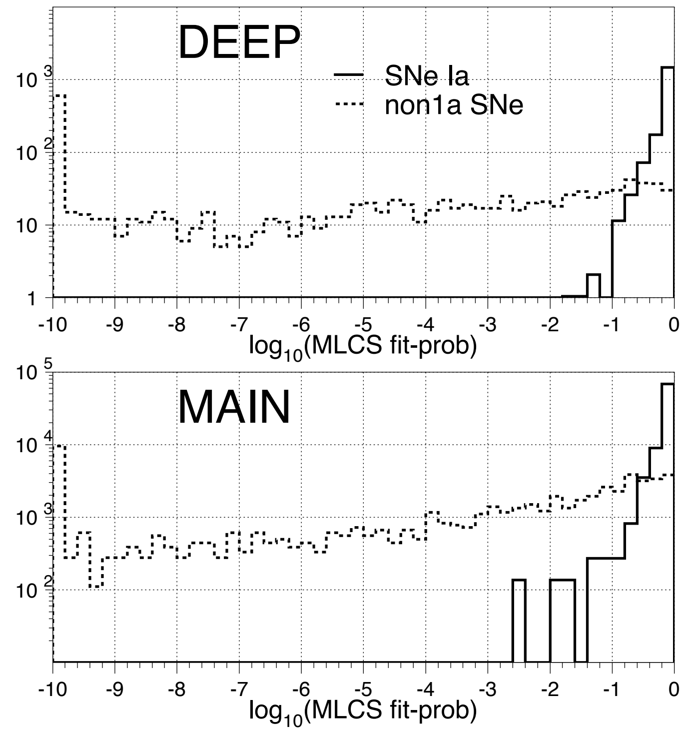

Figure 11.5: Demonstrating our ability to distinguish SNe Ia and core-collapse supernovae from light curve data alone. We fit each simulated SN Ia and SNcc light curve with an SN Ia model, and from the χ^2 of the fit, tabulated P_{χ^2}, the probability of getting a value of χ^2 larger than that value. Plotted is the distribution of values (note the logarithmic y-axis) for those objects that are true core-collapse SN (dashed line) and true SN Ia (solid line), for simulations of the deep drilling fields and the main survey fields. Cutting on high P_{χ^2} gives a clean SN Ia sample with little contamination.

SN Type	Relative Fraction of Core-Collapse SNe
IIP	0.70
Ib/c	0.15
IIL	0.10
IIn	0.05

Table 11.1: Assumed Distribution of Different Types of Core-Collapse Supernovae

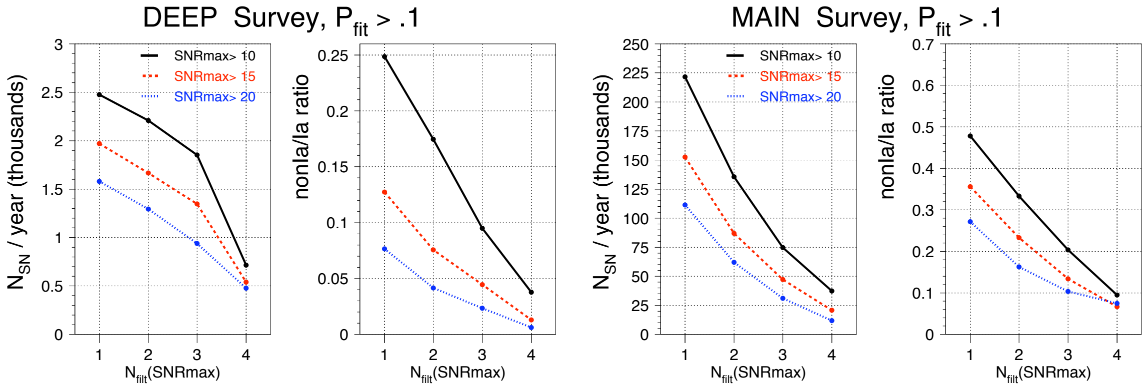

Figure 11.6: *Left*: Rates of Type Ia and Non-Ia supernovae are shown as a function of the number of filters passing S/N cuts plus P_{χ^2} >0.1 for the deep sample. *Right*: Same but for the main sample. Note that both samples use an assumed host galaxy spectroscopic redshift.

and core-collapse sample to templates using the SNe Ia MLCS2k2 model of Jha et al. (2007). Our hope is that the goodness of fit (as quantified in terms of the probability of observing a value of χ^2 greater than the measured value, P_{χ^2}) would be a clean way to distinguish the two classes of objects. This was borne out, as shown in Figure 11.5. The distributions of P_{χ^2} peaked sharply near $P_{\chi^2} = 1$ for SN Ia, and are very flat, extending to low probabilities for core collapse supernovae. Figure 11.6 is analogous to Figure 11.2, now showing the number of SNe Ia with an additional cut of $P_{\chi^2} > 0.1$, and the contamination rate. The main sample has 2–3 times more contamination due to the sparser light curves. Figure 11.7 shows the redshift distributions for the deep and main samples, for the SNe Ia and different types of core collapse supernovae. The contamination with our assumptions is dominated by SNe Ib/c, with the bright SNe IIn contributing at large redshift.

Improvements in our knowledge of the fraction of Type Ib/c supernovae would help us better understand the overall contamination of the LSST SN Ia sample. The LSST SN Ia supernova cosmology samples will have some level of core collapse contamination, and minimizing and understanding that contamination is important for precision cosmology.

11.4 SN Ia Photometric Redshifts

Scot S. Olivier, Sergei Nikolaev, Willem H. de Vries, Kem H. Cook, S. J. Asztalos

Supernova cosmology is currently based on measurements of two observable SN Ia quantities: the brightness at several epochs (light curve) observed in one or more bands and the redshift of features in the spectrum of the supernova (or the host galaxy).

Only a small fraction of the SNe Ia discovered by LSST will have spectroscopic measurements of redshift. Instead the redshift determination for most of these SNe Ia will be based on photometric measurements of the broad-band colors from either the host galaxy or the SN. Redshift determinations of galaxies, for which spectroscopy was unavailable, have been estimated based on their colors (§ 3.8). This type of "photometric redshift" can also be used for SNe Ia (Barris et al. 2004; Wang 2007; Wang et al. 2007).

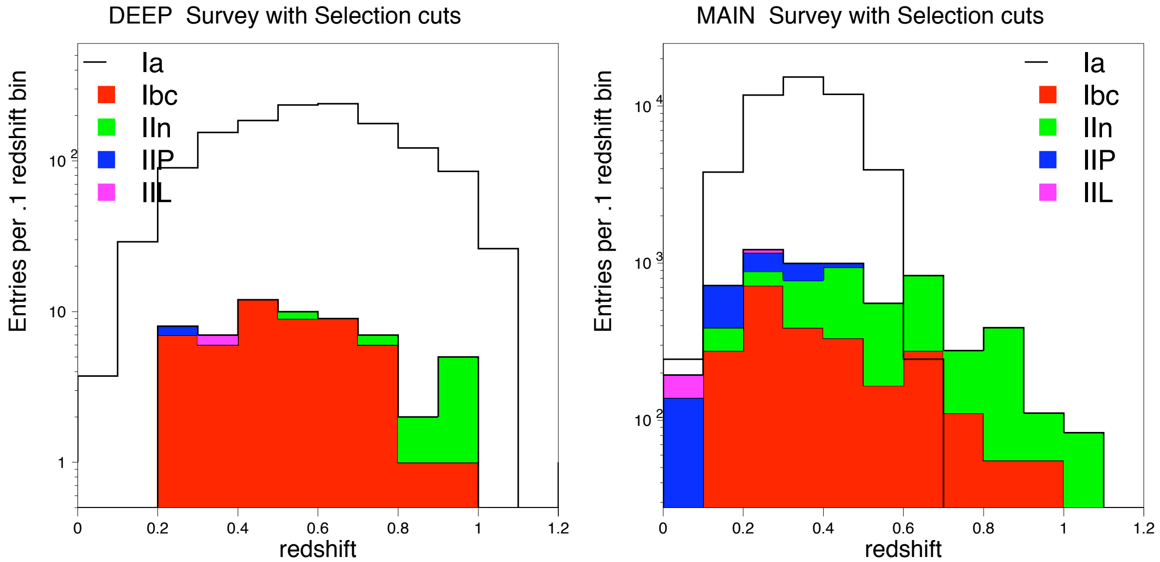

Figure 11.7: *Left*: Rates of Type Ia and Non-Ia supernovae are shown as a function of the redshift for the deep sample. *Right*: Same but for the main sample. Note that both samples use an assumed host galaxy spectroscopic redshift.

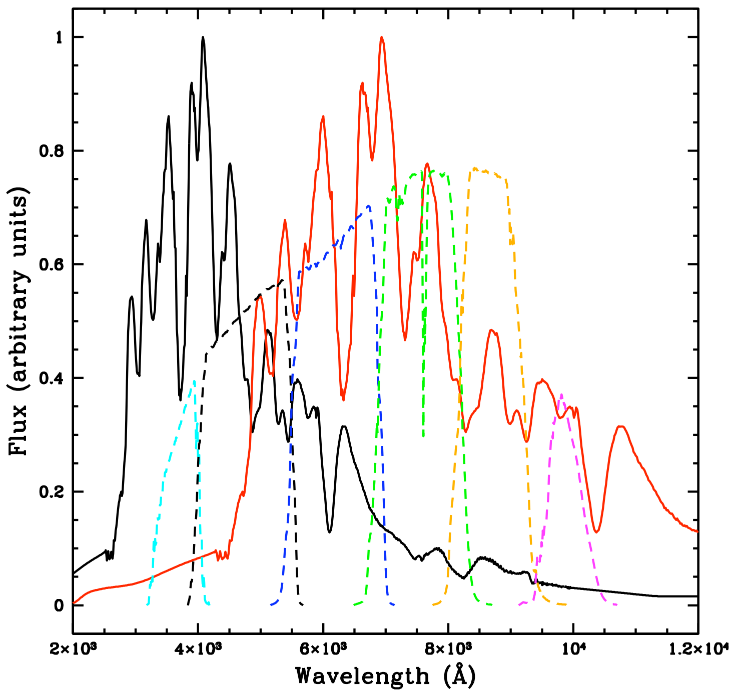

Figure 11.8: High quality SN Ia spectra at $z = 0$ (black) and $z = 0.7$ (red) overlaid with the LSST filter bands. The observed relative intensity in each filter (i.e., the colors) can be used to estimate the redshift.

SN Ia spectra are characterized by broad emission and absorption features. Figure 11.8 shows a nominal SN Ia spectrum at two redshifts along with the wavelength bands for the LSST filters. If the intrinsic spectrum is known a priori, the colors have the potential to accurately determine the redshift. Errors in this redshift estimate will be introduced by noise in the photometric measurements, variability in the intrinsic spectrum, degeneracies in the redshift determination, and uncorrected extinction due to dust along the line of sight. Since SN Ia spectra evolve in time, errors in the redshift estimate are also introduced by imprecise knowledge of the epoch of observation relative to the time of the explosion. However, this time evolution also provides an opportunity to use observations at multiple epochs in order to improve the redshift estimation.

Figure 11.9 shows the evolution of SN Ia spectra as well as their variability limits as a function of stretch and rest-frame epoch. For each stretch-epoch bin, the average spectrum was derived by co-adding SN Ia "normal" spectra from the literature (e.g., Jha et al. 2006; Matheson et al. 2008; Foley et al. 2008). The spectra can be calibrated to absolute flux units by comparing to the actual measured magnitudes of Type Ia (after the latter have been corrected for reddening and standardized based on the observed stretch). Focusing on the variability of spectra derived from real supernovae allows for more realistic simulations of supernovae observed by LSST.

The LSST SN Science Team is currently studying the accuracy with which the redshifts of SNe Ia can be estimated using the broadband photometry provided by the LSST observations. The approach is based on simulating the supernovae using the methods described in § 11.2.

The redshift of the supernova is then another free parameter in a model which includes the stretch and intrinsic color of the SN light curve and the dust extinction (de Vries et al. 2009). This procedure does not use the apparent brightness as an indicator of redshift, but uses the shape and color of the light curve as it evolves over time and across different passbands. Therefore, it is sensitive to the $(1 + z)$ time dilation effect which, like a spectroscopic redshift, provides a distance-modulus independent measurement.

Fitting the light curve of each model supernova gives the estimate of the photometric redshift and stretch, which can be compared to the original values used in generating the supernova. Figure 11.10 shows the accuracy of the photometric redshift and stretch determination based on simulation of 100 SNe Ia. These SNe Ia were selected uniformly from $z = [0, 1]$, stretch $s = [0.86, 1.16]$, and randomly across the LSST sky. Each SN Ia light curve was then propagated through the results of the Operations Simulator (§ 3.1) and photometric uncertainties were applied according to the LSST exposure time calculator (§ 3.2). The light curves were then fit with the photometric redshift fitting code.

In the figure, we turned off the effects of reddening and the variability in the Type Ia spectra. Reddening in particular will have an important impact of our ability to recover photometric redshift. If $R_V = 3.1$ as in the Milky Way, we will be able to calibrate out the effect of reddening on redshift determination to an accuracy of a percent in $(1 + z)$, but if the reddening law is unconstrained, one might get biases in estimated $(1 + z)$ at the few percent level.

This is explored in a bit more detail in Figure 11.11, which focuses on the deep drilling fields; the ability to recover photometric redshift, distance modulus, and reddening (again assuming a fiducial value for R_V) from our light curves is shown.

Although initial results quantifying the accuracy of photometric redshifts for SNe Ia are promising, more work is needed in order to fully understand the effect of photometric errors and intrinsic spectral variability, as well as inaccuracies in the spectral templates and incompleteness in the light curve sampling.

11.5 Constraining the Dark Energy Equation of State

Philip A. Pinto, Peter Garnavich, W. Michael Wood-Vasey, Rahul Biswas, Benjamin D. Wandelt

Type Ia supernovae (SNe Ia) are the best standard candles at large distances (Gibson et al. 2000; Parodi et al. 2000). Supernovae provided the first of the triad of observational constraints on which the now-standard dark energy-dominated model of cosmology is based (Riess et al. 1998; Perlmutter et al. 1999). The challenge of the next decade of supernova research is to explore the physics of supernovae themselves, their relationship with their environments, and the nature of the redshift-luminosity relation for SNe Ia. Massive samples of supernovae at all redshifts with superb data are required for these goals. As we have seen in § 11.2, the LSST data will produce on the order of 50,000 SNe Ia per year with photometry good enough for accurate light curve fitting. The sample will have a mean redshift of $z \sim 0.45$, stretching up to $z \sim 0.8$.

Supernova color statistics and good light curves, combined with a relatively small number ($\sim 1\%$) of sample spectra, will reveal any dependence of the supernova standard candle relation on parameters other than light curve shape and extinction, shedding light on any systematic errors in the SN Ia technique.

The large number of supernovae detected allows for a number of different approaches. Rough models show that even $\sim 10,000$ SNe Ia with intrinsic scatter in the distance indicator of 0.12 mag can constrain a constant equation of state w for a flat cosmology to better than 10% with no additional priors (Figure 11.12). Over 10 years one should thus have ~ 50 independent measurements of w, each to 10%. This of course assumes that there is no systematic floor in the supernova distance determination. With such a large sample, we could imagine deriving w independently for subsamples of supernovae with identical properties (e.g., light curve decay times, host galaxy types, etc.), to look for such systematics. Each subclass will provide an independent estimate of w, and consistency will indicate lack of serious systematic effects such as supernova evolution (§ 11.7).

With a sample of 50,000 SNe Ia (i.e., about one tenth of the full sample LSST will gather in ten years), one can put constraints better than 5% on a constant dark energy equation of state w (Appendix A). With a redshift-dependent equation of state, these data will constrain w_0 to 0.05, and w_a to accuracy of order unity (Figure 11.13).

With weak lensing (Chapter 14), constraining cosmological parameters requires a model for the growth of structure with epoch. By contrast, SN Ia luminosity distances constrain cosmology by directly measuring the redshift-distance relation, and therefore the metric itself. If dark energy is a manifestation of something radically new in space-time gravity, a comparison of the two approaches will reveal discrepancies, which will give us clues about this new physics.

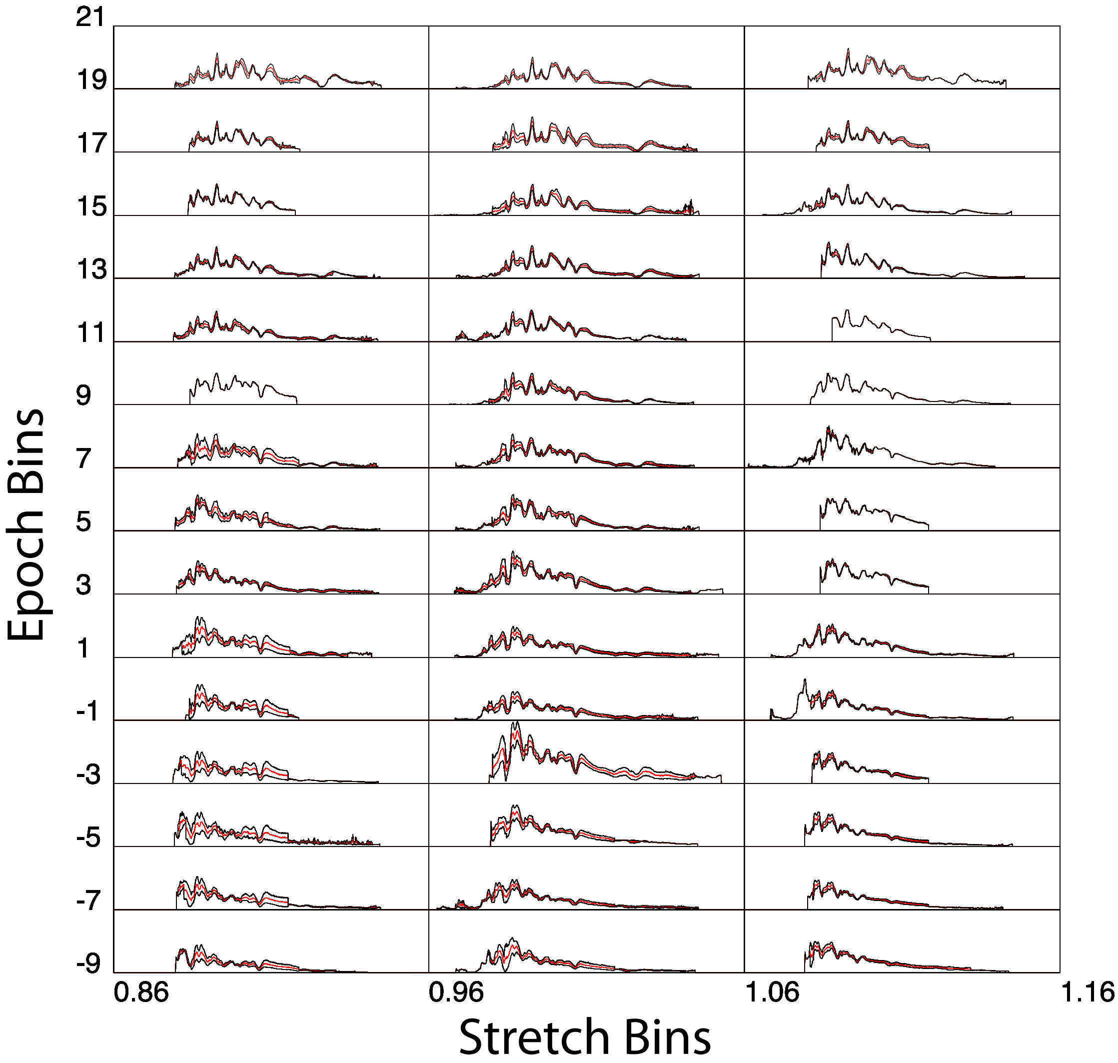

Figure 11.9: SN Ia spectra and their variability limits in "stretch-rest frame epoch" space. Each bin shows the average rest-frame spectrum in relative units (red) and $\pm 1\sigma$ limits (black). The x and y labels indicate the bin boundaries in stretch and rest-frame epoch (in days); the wavelength scale within each bin is from $1,000$Å to $15,000$Å. A stretch factor of unity corresponds to a supernova whose light curve drops by 1.0 mag in 15 days in the B band (Jha et al. 2006).

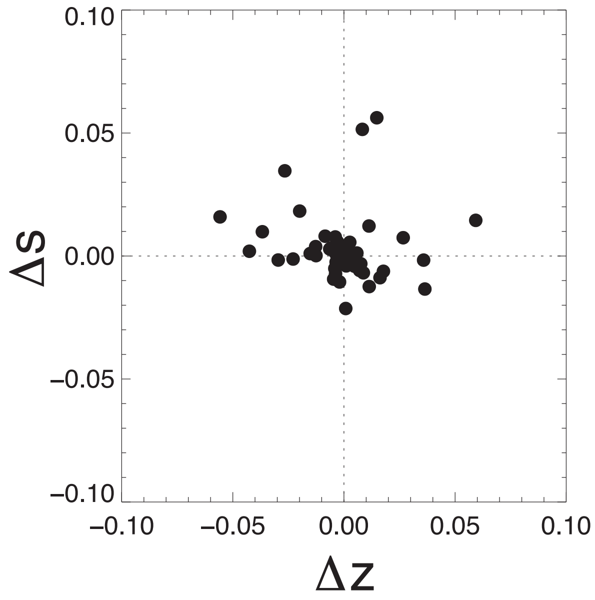

Figure 11.10: Recovery of spectroscopic redshifts and stretch using photometric information alone for 100 SNe Ia simulated from $0 < z < 1$, randomly populated across the LSST-visible sky, and propagated through the LSST Operations Simulator cadence for those fields. Milky Way reddening (with $R_V = 3.1$) is assumed here; the redshift determination is likely to be worse if this assumption is not valid.

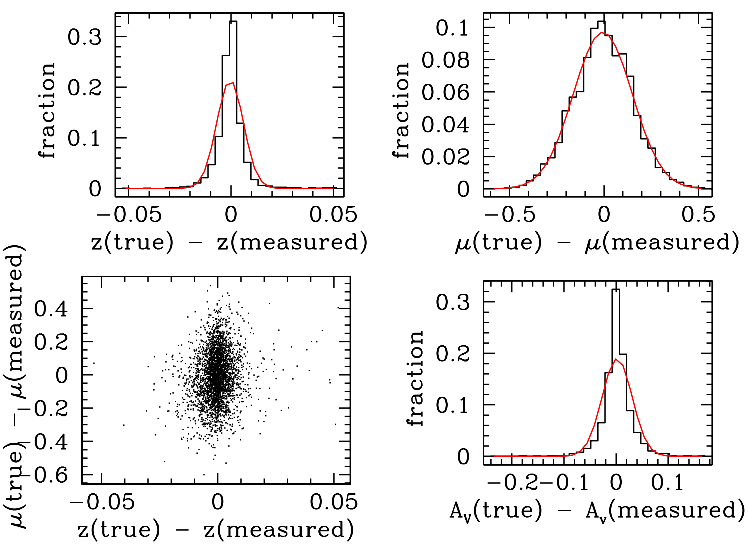

Figure 11.11: Simulations showing the errors in recovering $z < 1$ SN properties from light curves obtained in the deep-drilling mode. (clockwise from top left): 1) redshift errors; mean = −0.0004, $\sigma_z = 0.007$. 2) distance modulus μ error; mean = −0.006, $\sigma_\mu = 0.16$. 3) reddening error; mean = 0.002, $\sigma_{A_V} = 0.03$. 4) correlation between redshift and distance modulus errors. The covariance is weak.

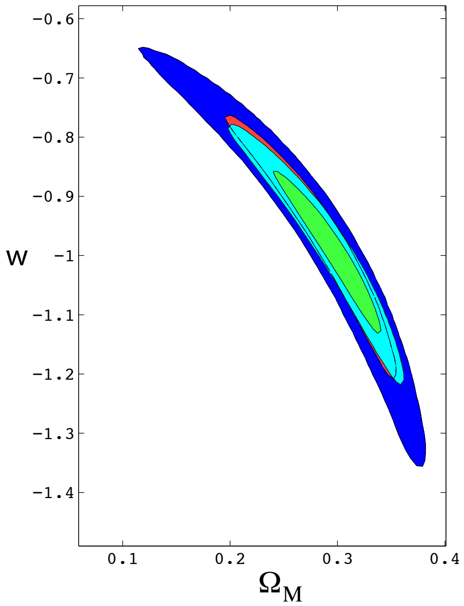

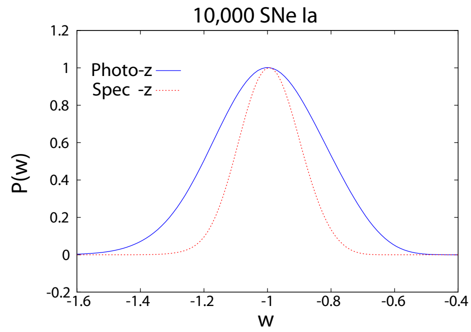

Figure 11.12: Forecasted constraints on a constant equation of state w in a flat cosmology from about 10,000 supernovae. The left panel shows the joint posterior distribution on Ω_m and w, assuming an intrinsic distribution in the distance indicator of 0.12 mag. The green and cyan contours show the 68% and 95% constraints when photometric redshifts are used, while the red and blue contours show the same constraints with spectroscopic redshifts. The right panel shows the constraints on w marginalized over Ω_M. Results are shown separately assuming that we have spectroscopic redshifts for all supernova hosts, and the more realistic case of photometric redshifts only. No other priors were used.

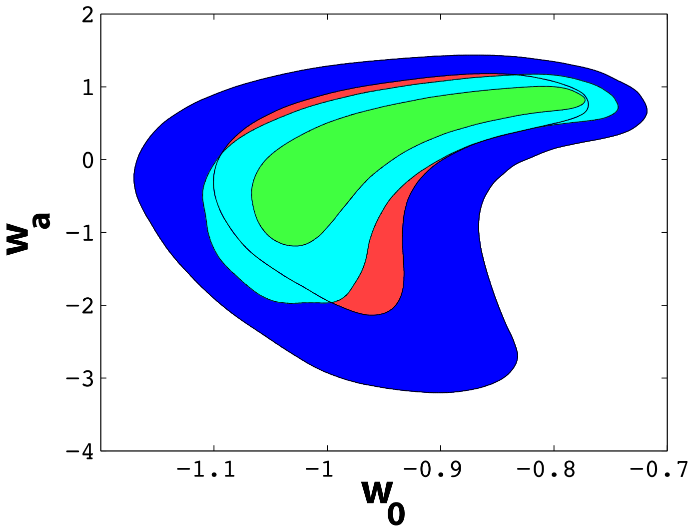

Figure 11.13: Forecast for joint posterior distribution on the parameters of a time evolving equation of state parametrized by $w(a) = w_0 + w_a(1 - a)$ in a flat cosmology from 50,000 supernovae (i.e., one year of the LSST survey). The green and cyan contours show the 68% and 95% constraints including photometric errors on redshift as a Gaussian with an error $\sigma_z = 0.01(1 + z)$, while the red and blue contours ignore photometric errors and only include an intrinsic dispersion of 0.12 mag in the distance indicator.

11.6 Probing Isotropy and Homogeneity with SNe Ia

W. Michael Wood-Vasey

The most basic cosmological question about dark energy is whether it is constant in space, time, and local gravitational potential (§ 15.4). One of the most powerful properties of SNe Ia as cosmological probes is that even a single object provides useful constraints.

For general cosmological investigations it will be possible to minimize various systematic difficulties inherent in the analysis of SNe Ia by calibrating the LSST SN Ia sample vs. other cosmological probes. But one can then start to determine whether the dark energy is uniform across space and time.

The all-sky nature of the sample of 500,000 SNe Ia that the LSST will identify in its 10 years of operations will enable searches for an angular dependence in the redshift-distance relation, thus determining whether the dark energy equation of state as characterized by w, and possibly even w_a, are directionally dependent. Any such signature would surely be an indication of fundamental new physics.

To investigate isotropy, one can divide up the LSST SNe Ia into 500 40 deg^2 pixels on the sky, each containing one thousand SNe Ia (Figure 11.14). Given the Hubble diagram for each pixel, one obtains 500 independent measures of w to look for variations which violate assumptions of isotropy and homogeneity: What is the rms for w over all the pixels? If there is variation in w, is it smoothly varying (i.e., correlated), and is the variance correlated with large-scale structure? These isotropy tests will be directly comparable to the large-scale structure maps that will come from galaxy photometric redshift surveys, weak lensing, and strong-lensing from clusters. Further explorations can be made by investigating shells of redshift and the correlation of SN Ia vs. local environment, both in galaxy properties and gravitational potential. See § 15.4 for further probes of the isotropy of dark energy.

11.7 SN Ia Evolution

David Cinabro, Saurabh W. Jha

One reason for a focus on SNe Ia is their observational homogeneity. When a small subset of peculiar SNe Ia are removed, easily identified by unusual colors at the peak of the light curve, the dispersion of SN Ia peak luminosities at rest-frame blue bands is about 20%, corresponding to 10% dispersion in distance. This is perfectly adequate for measurements of cosmological parameters with sample sizes of a few hundred. But without understanding the physical origins of this dispersion, and whether it has systematic effects that depend on redshift, we will not be able to use the full statistical power of the tens to hundreds of thousands of SNe Ia that LSST will find. Already the latest measurements of cosmology parameters with SNe Ia (Hicken et al. 2009; Kessler et al. 2009a) have uncertainties with significant contributions from systematic effects.

With such a large sample size it becomes possible to test for the underlying causes of the intrinsic dispersion of SN Ia peak luminosity. Dependence on cosmic time, or redshift, would most likely

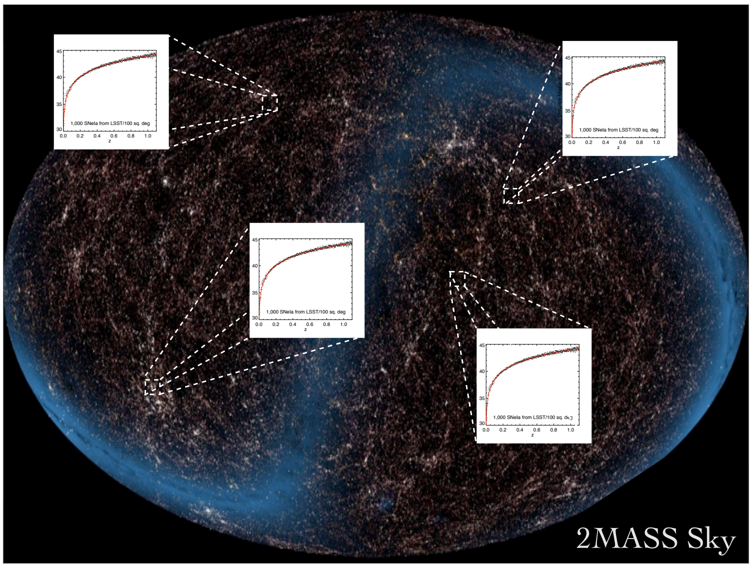

Figure 11.14: Testing the isotropy of dark energy by obtaining SN Ia luminosity-redshift measurements in each of 500 pixels on the sky. Each such pixel of 40 deg^2 will have on the order of 1000 SNe Ia, and cosmological parameters can be estimated from each of these independently. The background sky image is from the 2MASS survey, and shows the distribution of nearby galaxies.

indicate evolution of the SN Ia progenitor population. There is already good evidence for a difference in the properties of SNe Ia as a function of host galaxy type. Higher luminosity, slowly brightening, and slowly declining SNe Ia are preferentially associated with star-forming galaxies, while dimmer, fast brightening, and rapidly declining SNe Ia are preferentially in passive galaxies (Sullivan et al. 2006). At the present level of measurement, the two populations of supernovae follow the same correlation between light curve stretch and peak luminosity, but it is suggestive that more subtle effects may be associated with the SN Ia environment such as the host galaxy's historical development and properties such as metallicity. Indeed there is good evidence for a correlation between age, or metallicity, and SN Ia peak luminosities. In a study of 29 galaxy spectra that hosted SNe Ia, Gallagher et al. (2008) show that SN Ia peak luminosities are correlated with stellar population age and therefore metallicity as well. They also note a suggestive correlation between age, or metallicity, and residual on the Hubble diagram.

The effect is large, of the same order as the 20% intrinsic scatter, and validates theoretical models of the effect of population age, or metallicity, on SN Ia progenitor composition (Hoeflich et al. 1998; Umeda et al. 1999; Timmes et al. 2003). Given that stellar populations will naturally be younger in higher redshift supernovae, this could lead to a systematic effect as a function of redshift. Measurement of SN Ia evolution, or lack thereof, will provide valuable constraints on these models. LSST will allow correlations of supernovae properties with those of their host galaxies. For example, Howell et al. (2009) correlated SN Ia luminosities with host metallicities estimated from the host photometric colors, and Hicken et al. (2009) found that host morphology correlates with SN Ia extinction and scatter on the Hubble diagram. The large LSST sample would allow one to subdivide by galaxy properties, measuring cosmological parameters for each subsample separately.

Our lack of understanding of what SNe Ia progenitors really are (§ 11.8) limits our confidence in using them for cosmology at a precision level. We would like to understand the progenitors and explosion models that lead to both the intrinsic scatter of normal SN Ia properties and give rise to the peculiar population. Understanding the physical causes of peculiar SNe Ia, such as SN 2005hk (Sahu et al. 2008; Stanishev et al. 2007; Phillips et al. 2007; Chornock et al. 2006) and 2005gj (Hughes et al. 2007; Prieto et al. 2007; Aldering et al. 2006), has the promise to constrain models for normal SNe Ia and illuminate the underlying reason for the diversity of normal SNe Ia. We now have only a handful of truly peculiar objects, i.e., objects not well described by the family of light curves with one free parameter, because they are only a few percent of all SNe Ia. The LSST sample of SNe Ia will yield a larger sample of peculiar objects that can be targeted for further study.

11.8 SN Ia Rates

Evan Scannapieco, Benjamin Dilday, Saurabh W. Jha

There is now broad consensus that a Type Ia supernova is the thermonuclear explosion of a carbon-oxygen white dwarf star that accretes mass from a binary companion until it approaches the Chandrasekhar mass limit (e.g., Branch et al. 1995). However, much remains to be learned about the physics of SNe Ia, and there is active debate about both the nature of the progenitor systems and the details of the explosion mechanism. For example, the binary companion may be a main sequence, giant, or sub-giant star (the single-degenerate scenario), or a second white dwarf (the double-degenerate scenario). The type of the companion star determines in part the predicted time delay between the formation of the binary system and the SN event (Greggio 2005). The time delay can be constrained observationally by comparing the SN Ia rate as a function of redshift to the star formation history (Strolger et al. 2004; Cappellaro et al. 2007; Pritchet et al. 2008).

In order to test such a model for the evolution of the SN Ia rate, improved measurements of the rate as a function of redshift and of host galaxy properties are needed. The LSST is well suited to provide improved measurements of the SN Ia rate, with unprecedented statistical precision, and over a wide range of redshifts. Rate studies are much less sensitive to photometric redshift uncertainties than SN Ia cosmology measurements (e.g., Dilday 2009), and the vast photometric LSST SN Ia sample will be directly applicable to this problem.

The insight into the nature of the progenitor systems that SN Ia rate measurements provide can also potentially strengthen the utility of SNe Ia as cosmological distance indicators (§ 11.7). Although the strong correlation between SN Ia peak luminosity and light curve decline rate was found purely empirically (Pskovskii 1977; Phillips 1993), the physics underlying this relation has been extensively studied (Höflich et al. 1995, 1996; Kasen & Woosley 2007). There is hope that improved physical understanding and modeling of SNe Ia explosions, coupled with larger high-quality observational data sets, will lead to improved distance estimates from SNe Ia. As part of this program, deeper understanding of the nature of the progenitor systems can help narrow the range of initial conditions that need to be explored in carrying out the costly simulations of SNe Ia explosions that in principle predict their photometric and spectroscopic properties.

Measurement of the SN Ia rate may also have a more direct impact on the determination of systematic errors in SN Ia distance estimates. The empirical correlation discussed in § 11.7 between stretch parameter and stellar populations in the host (Hamuy et al. 1996; Howell 2001; van den Bergh et al. 2005; Jha et al. 2007) suggest connection between the age of the stellar population and the SN Ia rate, e.g., a "prompt" channel from progenitors found in star-forming regions and a "delayed" channel which depends perhaps only on the integrated star formation history of the host.

Mannucci et al. (2006), Scannapieco & Bildsten (2005), Neill et al. (2006), Sullivan et al. (2006), and Aubourg et al. (2008) have argued that a two-component model of the SN Ia rate, in which a prompt SN component follows the star formation rate and a second component follows the total stellar mass, is strongly favored over a single SN Ia channel. In this picture, since the cosmological star formation rate increases sharply with lookback time, the prompt component is expected to dominate the total SN Ia rate at high redshift. Mannucci et al. (2006) and Howell et al. (2007) pointed out that this evolution with redshift can be a potential source of systematic error in SN Ia distance estimates, if the two populations have different properties and are not properly disentangled.

To model the contributions of each of these two types of progenitors, Scannapieco & Bildsten (2005) write the total SN Ia rate as

$$\mathrm{Rate}_{\mathrm{Ia}}(t) = AM_\star(t) + B\dot{M}_\star(t) \tag{11.2}$$

Here the A-component or delayed component is proportional to the total stellar mass of the host, and the B-component or prompt component is proportional to the instantaneous star formation rate (as measured from model fits to the broad-band spectra energy distribution (SED) of the host). Sullivan et al. (2006) later measured these proportionality constants to be $A = 5.3 \pm 1.1 \times 10^{-14}\, M_\odot^{-1}\,\mathrm{yr}^{-1}$ and $B = 3.9 \pm 0.7 \times 10^{-4}\, M_\odot^{-1}$, and the large sample of SNe Ia from the LSST will clearly improve these error bars. However, pinning the prompt component to the instantaneous star formation rate is theoretically unpleasing since the formation time of a white dwarf is no less than 40 Myr. It is far more likely that the "prompt" component exhibits a characteristic short delay τ, namely,

$$\mathrm{Rate}_{\mathrm{Ia}}(t) = AM_\star(t) + B\dot{M}_\star(t-\tau) \tag{11.3}$$

Mannucci et al. (2006) proposed modeling the B-component as a Gaussian centered at 50 Myr, but the true value of this delay remains extremely uncertain. Recently, Fruchter et al. (2006) developed an observational method that constrains the properties of core-collapse SNe and gamma-ray bursts (GRBs). The method involves observing the spatial locations of SNe in their host galaxies and calculating the fraction of the total host galaxy light contained in pixels fainter than these locations. Transients associated with recent star-formation are systematically located in the brightest pixels, while transients arising from older stellar populations are anti-correlated with the brightest regions.

Raskin et al. (2008) carried out detailed modeling to interpret such data and proposed a modified pixel method that can be used to constrain the properties of SNe Ia progenitors. What is needed is a procedure that correlates SNe Ia with the properties of their immediate environment in the galaxy, rather than with the host as a whole. In a spiral host, the ideal method for constraining SNe Ia progenitors would be to measure the relative brightness of pixels within annuli. In this case, as the density wave of star formation moves around the annulus, SNe Ia would appear behind it at a characteristic surface brightness determined by the level to which a stellar population fades away before SNe Ia appear. However, observations are never ideal, and observing a single annulus of a spiral host is subject to complications such as spurs, knots, and gaps. The solution to this problem is the doughnut method, which builds directly on the method described in Fruchter et al. (2006). The idea is to expand an annulus radially by some small but appreciable radius, so as to encompass enough of the host's morphological peculiarities to have a good representative sample, yet narrow enough to represent local variations in the host light. In Raskin et al. (2009), this method was applied to SDSS images using a sample of 50 local SNe Ia, finding clear evidence that the delay time τ associated with the B component exceeds 200 Myr. In the LSST data set with $0.7''$ resolution, the method can be applied to SNe Ia hosts out to ~250 Mpc. This will give over 1,000 SNe Ia from the main LSST survey per year, which will be sufficient to map out the short-time distribution of SNe Ia in exquisite detail, providing strong constraints on the relationship between star formation and SN Ia production.

11.9 SN Ia BAO

Hu Zhan

Since SNe Ia explode in galaxies, they can, in principle, be used as the same tracer of the large-scale structure as their hosts to measure baryon acoustic oscillations (BAOs, see § 13.3 for details) in the power spectrum of their spatial distribution. Considerations for measuring BAO with SNe Ia are as follows.

- As described elsewhere in this chapter, SNe Ia have rich and time-varying spectral features, so that their photometric redshifts can be determined more accurately than galaxy photometric redshifts § 11.4, which compensates for the sparsity of the SN Ia sample for constraining dark energy. Indeed, within the same redshift range of $z < 0.8$, measuring BAO with the LSST SN Ia sample will place slightly tighter constraints on w_0 and w_a than the LSST galaxy BAO.
- The SN Ia sample has a very different selection function from conventional galaxy samples that are selected by luminosity or color. Hence, SN Ia BAO can provide a weak consistency check for galaxy BAO.
- SNe Ia are standardizable candles. The narrow range of the standardized SN Ia intrinsic luminosity reduces the effect of Malmquist-like biases and luminosity evolution, as seen in galaxy surveys.
- Although SN Ia BAO only places weak constraints on w, it can significantly improve the constraints from SN Ia luminosity distances of the same data, leading to results comparable to those of LSST WL two-point shear tomography. In other words, the extra information from SN Ia BAO can make LSST SNe Ia more competitive with other LSST probes.

For the BAO technique to be useful, one must survey a large volume uniformly at a sufficient sampling density. Although SN Ia events are rare, the spatial density of SNe Ia accumulated by LSST over several years will be comparable to the densities targeted for future spectroscopic galaxy BAO surveys. In its wide survey mode, LSST will obtain half a million SNe Ia over 20,000 deg^2 to redshift $z = 0.8$ (§ 11.2). Such a sample is capable of measuring the baryon signature in the SN Ia spatial power spectrum. The significance of detection, however, depends on the assumptions about cosmology. For example, the baryon signature has been detected at the $\sim 3\,\sigma$ level (constraining ω_m to 10%) from SDSS Luminous Red Galaxies, both spectroscopically (Eisenstein et al. 2005)

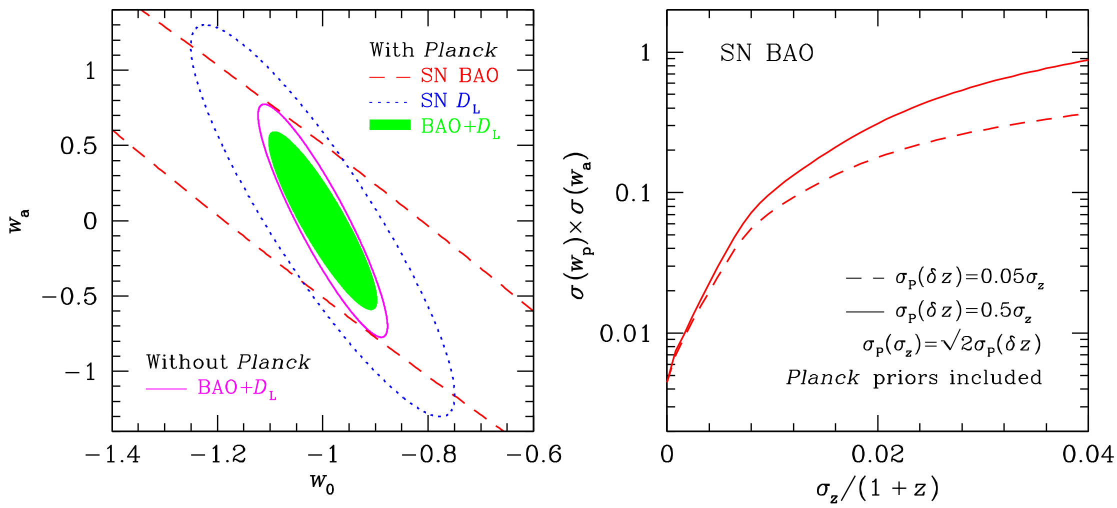

Figure 11.15: *Left panel*: Marginalized $1\,\sigma$ error contours of the dark energy EOS parameters w_0 and w_a from SN Ia BAO with Planck (dashed line), luminosity distances with Planck (dotted line), and the two combined with (shaded area) and without (solid line) Planck. The mean curvature parameter, Ω_k, is allowed to float. Even though results of the SN Ia BAO and SN Ia D_L techniques are sensitive to CMB priors individually, the combined result is much less so. *Right panel*: The error product $\sigma(w_p) \times \sigma(w_a)$ from LSST SN Ia BAO as a function of the rms photometric redshift error σ_z. The error $\sigma(w_p)$ equals the error on w_0 when w_a is held fixed. The priors on the photometric redshift biases are taken to be $0.5\sigma_z$ (solid lines) and $0.05\sigma_z$ (dashed lines), which correspond to calibrations with four and four hundred spectra per redshift bin, respectively, in the Gaussian case. To reduce the dimensions, we peg the prior on the photometric redshift rms to that on the photometric redshift bias: $\sigma_P(\sigma_z) = \sqrt{2}\sigma_P(\delta z)$. For comparison, LSST weak lensing, galaxy BAOs, and the two combined will achieve error products of ~ 0.01, 0.02, and 0.002, respectively (Zhan 2006). The behavior of the SN Ia BAO error product as a function of the photometric redshift rms is not specific to SNe Ia and is generally applicable to any photometric redshift BAO survey. Figure from Zhan et al. (2008), with permission.

and photometrically (Blake et al. 2007; Padmanabhan et al. 2007). These detections assume a flat Universe with a cosmological constant and a fixed scalar spectral index n_s. Under the same assumptions, LSST 20,000 deg^2 SN Ia BAO can constrain ω_m to 8% and ω_b to 15% (Zhan et al. 2008). If ω_b is fixed as well (as in Eisenstein et al. 2005), the same SN Ia BAO data can achieve $\sigma(\ln\omega_m) = 1.5\%$.

Dark energy constraints from SN Ia BAOs are much weaker than those from luminosity distances of the same SNe Ia, but these two techniques are highly complementary to each other. The left panel of Figure 11.15 illustrates that the combination of the two techniques improves the dark energy constraints significantly over those of luminosity distances, and the results are no longer sensitively dependent on CMB priors. The right panel of Figure 11.15 shows the degradation to dark energy constraints from LSST SN Ia BAO as a function of the photometric redshift rms and priors on the photometric redshift parameters. The slope of the error product changes around $\sigma_z \sim 0.01(1+z)$, because radial BAO information becomes available when photometric redshift errors are small enough.

11.10 SN Ia Weak Lensing

Yun Wang

The effect of weak lensing adds an additional uncertainty to using SNe Ia as cosmological standard candles at high redshift. Fluctuations in the matter distribution in our Universe deflect the light from SNe Ia, causing either demagnification or magnification (see, e.g., Kantowski et al. 1995; Branch & Khokhlov 1995; Frieman et al. 1997; Wambsganss et al. 1997; Holz 1998; Metcalf 1999; Wang 1999; Valageas 2000; Munshi & Jain 2000; Barber 2000; Premadi et al. 2001). The weak lensing effect of SNe Ia can be analytically modeled by a universal probability distribution function (UPDF) derived from the matter power spectrum (Wang 1999; Wang et al. 2002). Wang (2005) derived the observational signatures of weak lensing by convolving the intrinsic distribution in SN Ia peak luminosity, $p(L_{SN})$, with magnification distributions of point sources derived from the UPDF, $p(\mu)$. Figure 11.16 shows the difference between peak brightness and that predicted by the best-fit cosmological model for 63 SNe Ia with $0.5 \leq z \leq 1.4$ (top panels) and 47 SNe Ia with $0.02 \leq z \leq 0.1$ (bottom panels), taken from the data of Riess et al. (2004). The distribution of residuals of the low-z SNe Ia from current data is consistent with a Gaussian (in both flux and magnitude), while the high-z SNe Ia seem to show both signatures of weak lensing (high magnification tail and demagnification shift of the peak to smaller flux).

With hundreds of thousands of low- to medium-redshift SNe Ia from the LSST, and the thousands of high-redshift SNe Ia from the Joint Dark Energy Mission (JDEM), the error bars in the measured SN Ia peak brightness distributions at low, medium, and high redshifts will shrink by 1-2 orders of magnitude compared to the current data. This will enable us to rigorously study weak lensing effects on the SN Ia peak brightness distribution and derive parameters that characterize $p(L_{SN})$ and $p(\mu)$. Since SNe Ia are lensed by the foreground matter distribution, the large scale structure traced by galaxies in the foreground can be used to predict $p(\mu)$ directly, allowing us to cross-correlate with the $p(\mu)$ derived from the measured SN Ia brightness distributions.

The measured $p(\mu)$ is a probe of cosmology, since it is sensitive to the cosmological parameters (Figure 11.17) (Wang 1999). Thus the weak lensing of SNe Ia can be used to tighten constraints on cosmological parameters, and cross check the dark energy constraints from other LSST data (Wang 1999; Cooray & Caldwell 2006; Dodelson & Vallinotto 2006).

11.11 Core-Collapse Supernovae

Amy Lien, Brian D. Fields

The LSST will discover nearly as many Type II supernovae as Type Ia supernovae (§ 11.3) and will similarly obtain finely-sampled light curves in many colors. Core-collapse and Type Ia supernovae share very similar observational properties (light curve histories, maximum brightness), and thus the LSST strategies for optimizing Type Ia discovery will automatically discover an enormous number of core-collapse events. Indeed, the LSST will harvest core-collapse supernovae in numbers orders of magnitude greater than have ever been observed to date.

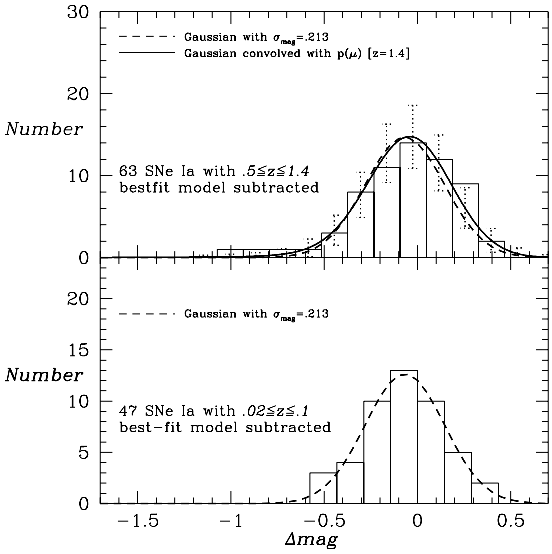

Figure 11.16: The distributions of fractional differences between the peak flux and that predicted by the best-fit model (Wang & Tegmark 2004) of 63 SNe Ia with $0.5 \leq z \leq 1.4$ (top panel) and 47 SNe Ia with $0.02 \leq z \leq 0.1$ (bottom panel). The weak lensing predictions are the solid lines in the top panels (with the error bars indicating the Poisson noise of these predictions), and depend on the assumption that the SN Ia intrinsic peak brightness distribution is Gaussian in flux. Figure used with permission from Wang (2005).

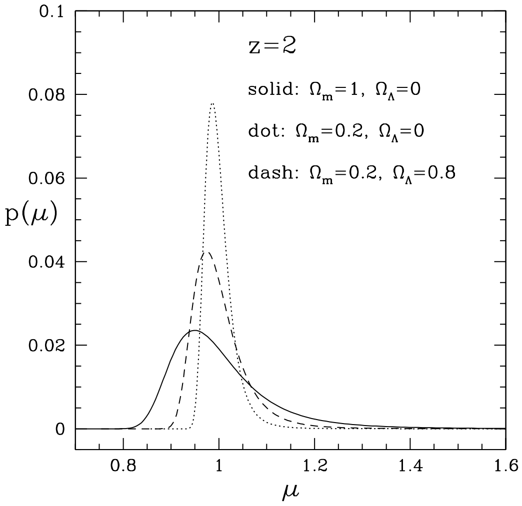

Figure 11.17: Magnification distributions of point sources for three different cosmological models at $z = 2$. Used with permission from Wang (1999).

Most SNe II can be distinguished from other types of SN by the duration and color evolution of their light curves. The supernova rates themselves, together with photometric redshifts which the LSST will obtain of their host galaxies (§ 3.8), will be a direct measure of the star formation history of the Universe. Late-time light curves will provide a direct measure of type II supernova ^{56}Ni (and hence iron) yields. The amount of iron which is released in the supernova explosion depends sensitively on the fraction of the total produced by explosive burning in the silicon shell that falls back into the compact object at the center. The watershed mass coordinate dividing what falls back from what escapes (the so-called "mass cut") can be measured from the ^{56}Ni yield, and is crucial for our understanding of cosmic chemical evolution of iron-group elements and the mass function of compact remnants.

The survey will map out the cosmic core-collapse supernova redshift distribution via direct *counting*, with very small statistical uncertainties out to a redshift depth that is a strong function of the survey limiting magnitude (§ 11.3; see also Lien & Fields 2009). Over all redshifts, the total annual harvest of core-collapse supernovae with one or more photometric points is predicted by Lien & Fields (2009) to be $\sim 3 \times 10^5$ events to $r = 23$.

The core-collapse supernova redshift history encodes rich information about cosmology, star formation, and supernova astrophysics and phenomenology; the large statistics of the supernova sample will be crucial to disentangle possible degeneracies among these issues. For example, the cosmic supernova rate can be measured to high precision out to $z \sim 0.5$ for all core-collapse types, and out to redshift $z \sim 1$ for Type IIn events if their intrinsic properties remain the same as those measured locally. Lien & Fields (2009) showed that in a single year of observation, LSST will determine the cosmic core-collapse supernova rate to an accuracy of 10% to $z \sim 0.9$.

A precise knowledge of the cosmic supernova rate would remove the cosmological uncertainties in the study of the wealth of observable properties of the cosmic supernova populations and their evolution with environment and redshift. Because of the tight link between supernovae and star formation, synoptic sky surveys will also provide precision measurements of the normalization and $z \leq 1$ history of cosmic star-formation rate in a manner independent of, and complementary to, current data based on UV and other proxies for massive star formation.

Furthermore, Type II supernovae can serve as distance indicators and would independently cross-check Type Ia distances measured in the same surveys (§ 11.12). Arguably the largest and least-controlled uncertainty in all of these efforts comes from the poorly understood evolution of dust obscuration of supernovae in their host galaxies; Lien & Fields (2009) outline a strategy to determine empirically the obscuration properties by leveraging large supernova samples over a broad range of redshift.

11.12 Measuring Distances to Type IIP Supernovae

Mario Hamuy

The subclass of Type II plateau supernovae can be used as distance indicators in a manner complementary to SNe Ia, although to smaller redshifts due their fainter intrinsic luminosities. The method is called the Expanding Photosphere Method (EPM) (Schmidt et al. 1994; Hamuy et al. 2001; Jones et al. 2009), and relies on the fact that the velocity of expansion of the photosphere (as measured from emission lines in the supernova spectrum) determines the size, and thus luminosity, of the photosphere. This technique needs at least two photometric observations over the first 50 days since discovery, using two optical filters (optimally in the $g - i$ range), as well as at least two spectroscopic observations contemporaneous to the photometric data in order to determine the photospheric expansion velocity as a function of time. Thus such work will require extensive access to 8-10-meter class telescopes with spectrographs. The calibration of the EPM is based on theoretical atmosphere models. Systematic differences in the two model sets available to date (Eastman et al. 1996; Dessart & Hillier 2005) lead to 50% differences in the EPM distances. However, once corrected to a common zero-point, both models produce relative distances with a 12% scatter (Jones et al. 2009), which reflects the internal precision of this technique. This is somewhat higher than the 7-10% internal precision that characterizes the techniques based on Type Ia supernovae. Since only relative distances are required for the determination of cosmological parameters, the thousands of Type II supernovae that LSST will discover will enable a completely independent determination of cosmological parameters.

Type II plateau supernovae can also be used for the determination of distances using the SCM (Standardized Candle Method), which does not require a theoretical calibration (Hamuy & Pinto 2002; Nugent et al. 2006; Olivares & Hamuy 2007; Poznanski et al. 2009). This technique, which relies on an empirical correlation between expansion velocity and peak luminosity, requires observations through two filters (e.g., r and i), at least on two epochs toward the end of the plateau phase (Olivares & Hamuy 2007). Because this technique is based on an empirical luminosity-velocity relation, a minimum of one spectroscopic observation is needed (preferentially contemporaneous to the photometric data), although two spectra would be desirable. This method yields relative distances with a precision of 10-15% (Olivares & Hamuy 2007; Poznanski et al. 2009), thus offering a independent route to cosmological parameters.

While EPM employs early-time data and SCM requires late-time observations, the two techniques are independent of one another. Thus two independent and complementary Hubble diagrams will be produced from the same data set of Type II plateau events. Since these objects are very different from SNe Ia in their explosion physics and progenitors, these data will provide a valuable assessment of the potential systematic errors that may affect the distances obtained from SNe Ia.

Optical observations covering the first 100 days of evolution of the Type II plateau events will provide information to estimate their bolometric luminosities (Bersten & Hamuy 2009), plateau lengths, and luminosity function. Through a comparison with hydrodynamic models (Litvinova & Nadezhin 1985; Utrobin 2007), these observables can be converted into physical parameters such as explosion energy and progenitor mass. This information will provide important advances in our understanding of the progenitor stars that produce these supernovae and their explosion mechanisms.

11.13 Probing the History of SN Light using Light Echoes

Jeonghee Rho

The light from supernovae can be visible as scattered-light echoes centuries after the explosion, whereby light from the supernova (in our own Milky Way or nearby galaxies) scatters off interstellar dust. These are identified in wide-field difference imaging on timescales over which the supernova evolves (weeks). This has been used to identify the type of supernovae associated with supernova remnants. There are a few light echo measurements that have been carried out of LMC supernova remnants (Rest et al. 2005), and light curve constructions using light echoes have been done for a few objects in nearby galaxies (Rest et al. 2008). Searching for light echoes from historic Galactic SNe has been challenging because of the need for repeated deep wide-angle imaging. Echoes of Galactic supernova remnants were first found in the infrared in Cas A (Krause et al. 2005) with the Spitzer Space Telescope. Here the infrared "echo" is the result of dust absorbing the SN outburst light, being heated and then re-radiating at longer wavelengths. Optical follow-up observations revealed the directly scattered light echo of Cas A (Rest et al. 2008).

LSST offers excellent opportunities to find the structures and evolution of light echoes of supernova remnants both in the Milky Way and in nearby galaxies. The structures of echoes change on timescales of days, months, and years, allowing one to construct accurate light curves and to constrain the properties of the progenitors.

Constraints on the light curves and accurate masses of progenitors of young supernova remnants are important for understanding nucleosynthesis and dust formation in SNe. Many species of nucleosynthetic yields and dust emission are more easily observable in supernova remnants than in supernovae, because after the reverse shock encountered by the ejecta, both the ejecta and dust are sufficiently heated to emit in both optical and infrared wavelengths.

11.14 Pair-Production SNe

Evan Scannapieco, David Arnett

Pair-production supernovae (PPSNe; § 8.3.3) are the uniquely calculable result of non-rotating stars that end their lives in the 140–260 $M_\odot$ mass range (Heger & Woosley 2002). Their collapse and explosion result from an instability that generally occurs whenever the central temperature and density of a star moves within a well-defined regime (Barkat et al. 1967). While this instability arises irrespective of the metallicity of the progenitor star, PPSNe are expected only in primordial environments. In the present metal-rich Universe, it appears that stars this massive are never assembled, as supported by a wide range of observations (e.g. Figer 2005; Oey & Clarke 2005). However, molecular hydrogen is a relatively inefficient coolant, so under primordial conditions the fragmentation of primordial molecular clouds was likely to have been biased towards the formation of stars with very high masses (Nakamura & Umemura 1999; Abel et al. 2000; Schneider et al. 2002; Tan & McKee 2004). Indeed, because very massive stars are only loosely bound and they exhibit large line-driven winds which scale with metallicity as $Z^{1/2}$ or faster (Vink et al. 2001; Kudritzki 2002), 140–260 $M_\odot$ mass stars would quickly shed a large fraction of their gas unless they were extremely metal poor.

Scannapieco et al. (2005) calculated approximate PPSNe light curves, varying parameters to blanket the range of theoretical uncertainties and possible progenitor masses. These are shown in Figure 11.18, in which they are compared with SN Ia and core-collapse SN light curves. Despite enormous kinetic energies of $\sim 50 \times 10^{51}$ ergs, the peak optical luminosities of PPSNe are similar to those of other SNe, even falling below the luminosities of SNe Ia and SNe II in many cases. This is because the higher ejecta mass produces a large optical depth and most of the internal energy of the gas is converted into kinetic energy by adiabatic expansion (see, e.g., Arnett 1982). The colors of the PPSN curves are also similar those to more usual SNe.

Thus distinguishing PPSNe from other SNe will require multiple observations that constrain the time evolution of these objects. In particular, there are two key features that are uniquely characteristic to PPSNe. The first is a dramatically extended intrinsic decay time, which is especially noticeable in the models with the strongest enrichment of CNO in the envelope. This is due to the long adiabatic cooling times of supergiant progenitors, whose radii are $\sim$ 20 AU, but whose expansion velocities are similar to, or even less than, those of other SNe. Second, PPSNe are the only objects that show an extremely late rise at times $\geq$ 100 days. This is due to energy released by the decay of ^{56}Co, which unlike in the SN Ia case, takes months to dominate over the internal energy imparted by the initial shock.

Such constraints will require an extremely long cadence, roughly 100 days in the rest frame, or $\sim$ 1 year for SNe at theoretically interesting redshifts $\geq$ 1. While the very faintest PPSNe, such as the 150 $M_\odot$ models in Figure 11.18 cannot be meaningfully constrained by LSST, co-adding the $\sim$ 16 images taken of each patch of sky each year in the z band will place exquisite constraints on 200 $M_\odot$ and 250 $M_\odot$ progenitor models. Indeed observations down to $z = 26.0$ covering 16,000 deg^2 will be able to detect thousands of $200 - 250 M_\odot$ PPSN if very massive metal-free stars make up even 0.01% of the stars formed at a redshift of 2, well within the range of theoretical uncertainties (Scannapieco et al. 2003; Jimenez & Haiman 2006; Tornatore et al. 2007). Even if very massive metal-free star formation does not occur below $z = 2$, hundreds of $z = 2-4$ PPSNe will be detected by LSST (Figure 11.19). At the same time such long-cadence studies will turn up large numbers of long duration SNe, such as the extremely bright SN 2006gy (Smith et al. 2007), which, while not likely to be of primordial origin, nevertheless will provide unique probes into extreme events in stellar evolution (§ 8.2.1).

11.15 Education and Public Outreach with Supernovae

W. Michael Wood-Vasey

Supernovae have always fascinated and engaged the public. The great wealth of supernovae that will come from a decade of LSST are an excellent opportunity to share the discoveries and science of LSST with the world. The hexa-color LSST movie of the sky leads to natural learning opportunities from elementary students through college and life-long learners. See Chapter 4 for a general discussion of EPO activities in the context of LSST. Here we focus on the unique engagement and educational opportunities related to supernova science.

Students can search for and study supernovae in the LSST data. From simple exercises in visual comparison, school children will learn that supernovae rise and fall in brightness and that they are associated with galaxies. This level of understanding is the perfect time to talk about brightness, cooling due to expansion, and radioactivity (the decay ^{56}Ni is the dominant source of energy after a week or two in a supernova). More advanced college students can learn about the image differencing, the expansion of the Universe, the life cycle of stars, and the surface brightness of

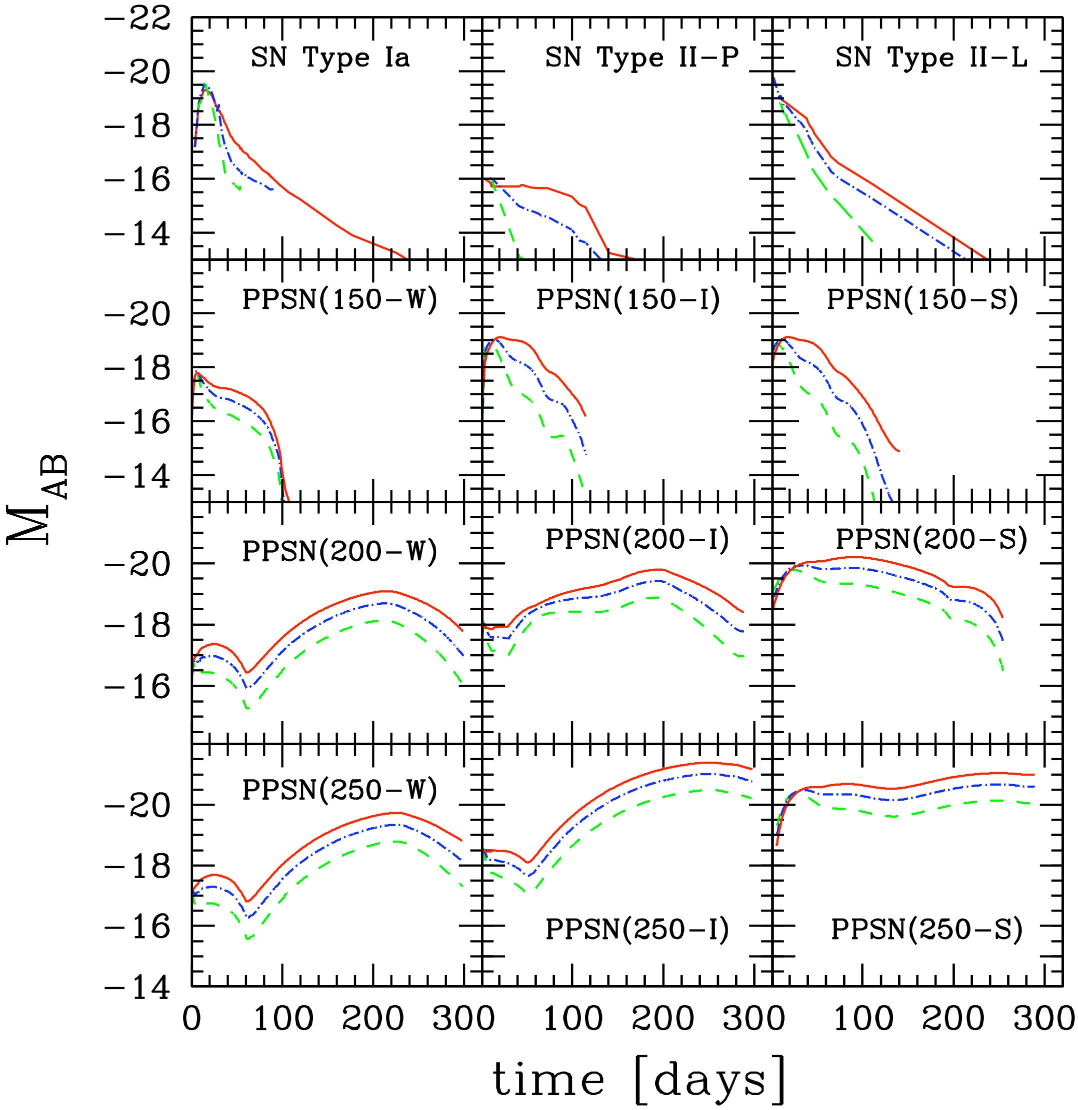

Figure 11.18: Comparison of light curves of a SN Ia, a SN IIp, a bright SN IIl, and PPSNe models with varying progenitor masses and levels of dredge-up. The models are labeled by the level of mixing from the core into the envelope (W-weak; I-Intermediate; S-Strong) and the mass of the progenitor star (150, 200, and 250 $M_\odot$). In all cases the solid lines are absolute V-band AB magnitudes, the dot-dashed lines are the absolute B-band AB magnitudes, and the dashed lines are the absolute U-band AB magnitudes. In general, less mixing leads to more ^{56}Ni production, which makes the SNe brighter at late times, while more mixing expands the envelope, which makes the SNe brighter at early times. Peak brightness also increases strongly with progenitor mass. Figure from Scannapieco et al. (2005), with permission.

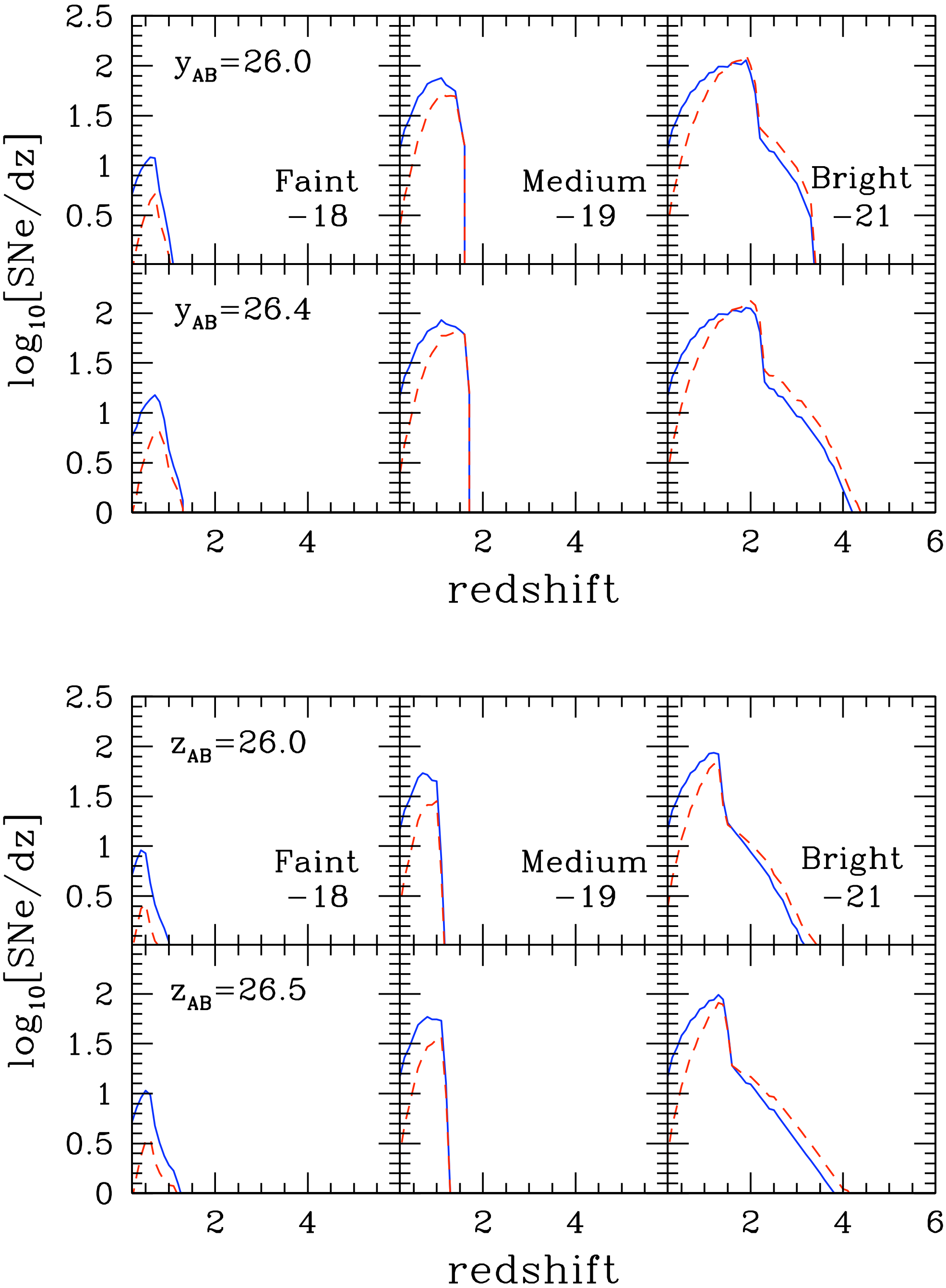

Figure 11.19: Number of PPSNe per unit redshift observable by LSST in y (top) and z (bottom) per unit redshift in a single 9.6 deg^2 field. Lines show models in which metal-free star formation occurs at a rate of 1% of the overall star-formation rate (red lines) or at a fixed rate of 0.001 $M_\odot\,\mathrm{yr}^{-1}\,\mathrm{Mpc}^{-3}$ (blue lines), assuming one PPSN per 1000 $M_\odot$ of metal-free stars formed.

expanding explosions. By measuring the light curve of a supernova, they will learn about measurement uncertainties and fitting data to empirical and analytic curves. Using the brightness of SNe Ia to measure the expansion of the Universe has already become a standard lab in astronomy courses. With LSST, each student could take their own patch of the Universe and compare with their classmates to learn about systematic errors, methods, techniques, and "global" measurements. More advanced opportunities to identify the type of supernovae based on their light curve properties could be effectively done either as individual labs or as a Supernova Zoo-type Citizen Science Project (c.f., the Palomar Transient Factory, http://www.astro.caltech.edu/ptf/ or Galaxy Zoo collaboration, http://www.galaxyzoo.org/) to benchmark and test the automated transient classification of LSST while teaching participants about redshift and time-dilation, color, luminosity, and every astronomer's favorite topic, extinction due to dust.

The basic scientific investigations that will be one of the important science topics for supernova science with LSST are extremely accessible. Do supernovae come from big galaxies or small? Are they close in to the center of galaxies or are they found in intra-cluster spaces? These topics will benefit from visual inspection and will teach basic concepts of sizes, projected distance, angles, as well as more advanced topics of cosmological distances, galaxy evolution, and metallicity.

The participation of the amateur/semi-professional astronomical community has always been a key aspect of time-domain astronomy. These opportunities will multiply a thousand-fold in the LSST era, and integration with robotic and individual telescopes and observing programs around the world will both share the LSST science with the world and significantly contribute to a number of the main LSST supernova science topics. By thoroughly examining the patterns of supernovae across the sky, students and the public can learn how supernovae match the distribution of galaxies and about the structure of the cosmos. At the most basic level, the general public and students will learn how the dramatic deaths of stars throughout the cosmos tells us about the fundamental nature of our Universe and the elements that make life possible.

References

Abel, T., Bryan, G. L., & Norman, M. L., 2000, *ApJ*, 540, 39
Aldering, G. et al., 2006, *ApJ*, 650, 510
Arnett, W. D., 1982, *ApJ*, 253, 785
Aubourg, É., Tojeiro, R., Jimenez, R., Heavens, A., Strauss, M. A., & Spergel, D. N., 2008, *A&A*, 492, 631
Barber, A. J., 2000, *MNRAS*, 318, 195
Barkat, Z., Rakavy, G., & Sack, N., 1967, *Phys. Rev. Lett.*, 18, 379
Baron, E., Nugent, P. E., Branch, D., & Hauschildt, P. H., 2004, *ApJL*, 616, L91
Barris, B. J. et al., 2004, *ApJ*, 602, 571
Bazin, G. et al., 2009, *A&A*, 499, 653
Bersten, M. C., & Hamuy, M., 2009, *ApJ*, 701, 200
Blake, C., Collister, A., Bridle, S., & Lahav, O., 2007, *MNRAS*, 374, 1527
Branch, D., & Khokhlov, A. M., 1995, *Phys. Rep.*, 256, 53
Branch, D., Livio, M., Yungelson, L. R., Boffi, F. R., & Baron, E., 1995, *PASP*, 107, 1019
Cappellaro, E., Botticella, M. T., & Greggio, L., 2007, in American Institute of Physics Conference Series, Vol. 937, Supernova 1987A: 20 Years After: Supernovae and Gamma-Ray Bursters, S. Immler, K. Weiler, & R. McCray, eds., pp. 198–205
Cappellaro, E., Evans, R., & Turatto, M., 1999, *A&A*, 351, 459
Chornock, R., Filippenko, A. V., Branch, D., Foley, R. J., Jha, S., & Li, W., 2006, *PASP*, 118, 722
Cooray, A., & Caldwell, R. R., 2006, *Phys. Rev. D*, 73, 103002

de Vries, W. et al., 2009, in preparation
Dessart, L., & Hillier, D. J., 2005, *A&A*, 439, 671
Di Carlo et al., 2002, *ApJ*, 573, 144
Dilday, B., 2009, in preparation
Dilday, B. et al., 2008, *ApJ*, 682, 262
Dodelson, S., & Vallinotto, A., 2006, *Phys. Rev. D*, 74, 063515
Eastman, R. G., Schmidt, B. P., & Kirshner, R., 1996, *ApJ*, 466, 911
Eisenstein, D. J. et al., 2005, *ApJ*, 633, 560
Figer, D. F., 2005, *Nature*, 434, 192
Foley, R. J. et al., 2008, *ApJ*, 684, 68
Frieman, J. A. et al., 1997, in The Evolution of the Universe: report of the Dahlem Workshop on the Evolution of the Universe, G. Borner & S. Gottlober, eds., p. 141
Fruchter, A. S. et al., 2006, *Nature*, 441, 463
Gallagher, J. S., Garnavich, P. M., Caldwell, N., Kirshner, R. P., Jha, S. W., Li, W., Ganeshalingam, M., & Filippenko, A. V., 2008, *ApJ*, 685, 752
Gibson, B. K. et al., 2000, *ApJ*, 529, 723
Gilliland, R. L., Nugent, P. E., & Phillips, M. M., 1999, *ApJ*, 521, 30
Greggio, L., 2005, *A&A*, 441, 1055
Guy, J. et al., 2007, ArXiv Astrophysics e-prints, astro-ph/0701828
Hamuy, M., Phillips, M. M., Suntzeff, N. B., Schommer, R. A., Maza, J., Smith, R. C., Lira, P., & Aviles, R., 1996, *AJ*, 112, 2438
Hamuy, M., & Pinto, P. A., 2002, *ApJL*, 566, L63
Hamuy, M. et al., 2001, *ApJ*, 558, 615
—, 2002, *AJ*, 124, 417
Heger, A., & Woosley, S. E., 2002, *ApJ*, 567, 532
Hicken, M., Wood-Vasey, W. M., Blondin, S., Challis, P., Jha, S., Kelly, P. L., Rest, A., & Kirshner, R. P., 2009, ArXiv e-prints, 0901.4804
Hoeflich, P., Wheeler, J. C., & Thielemann, F. K., 1998, *ApJ*, 495, 617
Höflich, P., Khokhlov, A., Wheeler, J. C., Phillips, M. M., Suntzeff, N. B., & Hamuy, M., 1996, *ApJL*, 472, L81
Höflich, P., Khokhlov, A. M., & Wheeler, J. C., 1995, *ApJ*, 444, 831
Holz, D. E., 1998, *ApJL*, 506, L1
Howell, D. A., 2001, *ApJL*, 554, L193
Howell, D. A. et al., 2009, *ApJ*, 691, 661
Howell, D. A., Sullivan, M., Conley, A., & Carlberg, R., 2007, *ApJL*, 667, L37
Hughes, J. P., Chugai, N., Chevalier, R., Lundqvist, P., & Schlegel, E., 2007, *ApJ*, 670, 1260
Jha, S. et al., 2006, *AJ*, 131, 527
Jha, S., Riess, A. G., & Kirshner, R. P., 2007, *ApJ*, 659, 122
Jimenez, R., & Haiman, Z., 2006, *Nature*, 440, 501
Jones, M. I. et al., 2009, ArXiv e-prints, 0903.1460
Kantowski, R., Vaughan, T., & Branch, D., 1995, *ApJ*, 447, 35
Kasen, D., & Woosley, S. E., 2007, *ApJ*, 656, 661
Kessler, R. et al., 2009a, ArXiv e-prints, 0908.4274
—, 2009b, *PASP*, 121, 1028
Krause, O. et al., 2005, *Science*, 308, 1604
Kudritzki, R. P., 2002, *ApJ*, 577, 389
Lien, A., & Fields, B. D., 2009, *Journal of Cosmology and Astro-Particle Physics*, 1, 47
Litvinova, I. Y., & Nadezhin, D. K., 1985, *Soviet Astronomy Letters*, 11, 145
Mannucci, F., Della Valle, M., & Panagia, N., 2006, *MNRAS*, 370, 773
Mannucci, F., Della Valle, M., Panagia, N., Cappellaro, E., Cresci, G., Maiolino, R., Petrosian, A., & Turatto, M., 2005, *A&A*, 433, 807
Matheson, T. et al., 2008, *AJ*, 135, 1598
Metcalf, R. B., 1999, *MNRAS*, 305, 746
Munshi, D., & Jain, B., 2000, *MNRAS*, 318, 109
Nakamura, F., & Umemura, M., 1999, *ApJ*, 515, 239
Neill, J. D. et al., 2006, *AJ*, 132, 1126
Nugent, P., Kim, A., & Perlmutter, S., 2002, *PASP*, 114, 803

Nugent, P. et al., 2006, *ApJ*, 645, 841

Oey, M. S., & Clarke, C. J., 2005, in Astrophysics and Space Science Library, Vol. 327, The Initial Mass Function 50 Years Later, E. Corbelli, F. Palla, & H. Zinnecker, eds., Springer, Dordrecht, p. 187

Olivares, F., & Hamuy, M., 2007, in VI Reunion Anual Sociedad Chilena de Astronomia (SOCHIAS), p. 40

Padmanabhan, N. et al., 2007, *MNRAS*, 378, 852

Parodi, B. R., Saha, A., Sandage, A., & Tammann, G. A., 2000, *ApJ*, 540, 634

Perlmutter, S. et al., 1999, *ApJ*, 517, 565

Phillips, M. M., 1993, *ApJL*, 413, L105

Phillips, M. M. et al., 2007, *PASP*, 119, 360

Poznanski, D. et al., 2009, American Astronomical Society Meeting Abstracts, Vol. 213, The Standard Candle Method For Type II-P Supernovae - New Sample And PTF Perspective. p. 469.09

Premadi, P., Martel, H., Matzner, R., & Futamase, T., 2001, *ApJS*, 135, 7

Prieto, J. L. et al., 2007, ArXiv e-prints, 0706.4088

Pritchet, C. J., Howell, D. A., & Sullivan, M., 2008, *ApJL*, 683, L25

Pskovskii, I. P., 1977, *Soviet Astronomy*, 21, 675

Raskin, C., Scannapieco, E., Rhoads, J., & Della Valle, M., 2008, *ApJ*, 689, 358

—, 2009, *ApJ*, submitted

Rest, A. et al., 2005, *ApJ*, 634, 1103

—, 2008, *ApJL*, 681, L81

Richardson, D., Branch, D., Casebeer, D., Millard, J., Thomas, R. C., & Baron, E., 2002, *AJ*, 123, 745

Riess, A. G. et al., 1998, *AJ*, 116, 1009

—, 2004, ArXiv Astrophysics e-prints, astro-ph/0402512

Sahu, D. K. et al., 2008, *ApJ*, 680, 580

Scannapieco, E., & Bildsten, L., 2005, *ApJL*, 629, L85

Scannapieco, E., Madau, P., Woosley, S., Heger, A., & Ferrara, A., 2005, *ApJ*, 633, 1031

Scannapieco, E., Schneider, R., & Ferrara, A., 2003, *ApJ*, 589, 35

Schmidt, B. P. et al., 1994, *AJ*, 107, 1444

Schneider, R., Ferrara, A., Natarajan, P., & Omukai, K., 2002, *ApJ*, 571, 30

Smith, N. et al., 2007, *ApJ*, 666, 1116

Stanishev, V. et al., 2007, in American Institute of Physics Conference Series, Vol. 924, The Multicolored Landscape of Compact Objects and Their Explosive Origins, T. di Salvo, G. L. Israel, L. Piersant, L. Burderi, G. Matt, A. Tornambe, & M. T. Menna, eds., pp. 336–341

Strolger, L.-G. et al., 2004, *ApJ*, 613, 200

Sullivan, M. et al., 2006, *ApJ*, 648, 868

Tan, J. C., & McKee, C. F., 2004, *ApJ*, 603, 383

Timmes, F. X., Brown, E. F., & Truran, J. W., 2003, *ApJL*, 590, L83

Tornatore, L., Ferrara, A., & Schneider, R., 2007, *MNRAS*, 382, 945

Umeda, H., Nomoto, K., Kobayashi, C., Hachisu, I., & Kato, M., 1999, *ApJL*, 522, L43

Utrobin, V. P., 2007, *A&A*, 461, 233

Valageas, P., 2000, *A&A*, 354, 767

van den Bergh, S., Li, W., & Filippenko, A. V., 2005, *PASP*, 117, 773

Vink, J. S., de Koter, A., & Lamers, H. J. G. L. M., 2001, *A&A*, 369, 574

Wambsganss, J., Cen, R., Xu, G., & Ostriker, J. P., 1997, *ApJL*, 475, L81

Wang, Y., 1999, *ApJ*, 525, 651

—, 2005, *Journal of Cosmology and Astro-Particle Physics*, 3, 5

—, 2007, *ApJL*, 654, L123

Wang, Y., Holz, D. E., & Munshi, D., 2002, *ApJL*, 572, L15

Wang, Y., Narayan, G., & Wood-Vasey, M., 2007, *MNRAS*, 382, 377

Wang, Y., & Tegmark, M., 2004, *Phys. Rev. Lett.*, 92, 241302

Wood-Vasey, W. M. et al., 2009, American Astronomical Society Meeting Abstracts, Vol. 213, Cosmology, Clusters, and Chemistry: How Supernovae Trace and Shape The Universe. p. 460.16

Zhan, H., 2006, *Journal of Cosmology and Astro-Particle Physics*, 8, 8

Zhan, H., Wang, L., Pinto, P., & Tyson, J. A., 2008, *ApJL*, 675, L1